UNIVERSIDADE FEDERAL DO CEARÁ

CENTRO DE CIÊNCIAS

PROGRAMA DE PÓS-GRADUAÇÃO EM QUÍMICA

LUCAS LIMA BEZERRA

COMPUTATIONAL ANALYSIS OF CO_2 CAPTURE THROUGH DEEP EUTECTIC SOLVENTS AND SILVER NANOPARTICLES

FORTALEZA

2026

LUCAS LIMA BEZERRA

COMPUTATIONAL ANALYSIS OF CO_2 CAPTURE THROUGH DEEP EUTECTIC SOLVENTS AND SILVER NANOPARTICLES

Tese apresentada ao Programa de Pós-Graduação em Química da Universidade Federal do Ceará como requisito parcial à obtenção do título de Doutor em Química. Área de concentração: Físico-Química.

Orientador: Prof. Dr. Norberto de Kássio Vieira Monteiro.
Coorientadora: Profa. Dra. Adriana Nunes Correia

FORTALEZA
2026

LUCAS LIMA BEZERRA

COMPUTATIONAL ANALYSIS OF CO_2 CAPTURE THROUGH DEEP EUTECTIC SOLVENTS AND SILVER NANOPARTICLES

Tese apresentada ao Programa de Pós-Graduação em Química da Universidade Federal do Ceará como requisito parcial à obtenção do título de Doutor em Química. Área de concentração: Físico-Química.

Aprovado em: 30/01/26.

BANCA EXAMINADORA

Prof. Dr. Norberto de Kássio Vieira Monteiro (Orientador)
Universidade Federal do Ceará (UFC)

Profa. Dra. Adriana Nunes Correia (Coorientadora)
Universidade Federal do Ceará (UFC)

Prof. Dr. Pierre Basílio Almeida Fechine
Universidade Federal do Ceará (UFC)

Prof. Dr. Ámison Rick Lopes da Silva
Universidade Federal do Vale do São Francisco (UNIVASF)

Profa. Dra. Simone Barreira Morais
Instituto Superior de Engenharia do Porto (ISEP)

To God

To my family and friends.

ACKNOWLEDGMENTS

Initially, I thank God for giving me health, wisdom, and willpower. I also thank my parents and sister for all their support and help in this crucial step in my academic life. Even in difficult times, you were always on my side and did not discourage me when major obstacles arose during my doctorate. You are so awesome!

To all my friends that I made during these six years in the Theoretical Chemistry Group: Leonardo Paes, Renato Veríssimo, Marcus Vinícius, Gizele Nascimento, Laudenor Amorim, Osmar Júnior, Lucas Coutinho, Ámison Rick, and Pabllo Abreu. Thank you for all the scientific and other unscientific debates.

I would like to thank my friends from Portugal, especially Vitória Dibo, Ana Luiza, Petra Albuquerque, Luiz Henrique, and Sandra Lavandeira, for all their laughter and support. Thank you so much! I also thank Professor Dra. Simone Barreira Morais accepted me into your research group, as well as for the availability and support before, during, and after my PhD visit to Portugal!

I would like to thank Professor Dr. Norberto de Kássio Vieira Monteiro for his patience, dedication, and professionalism, as well as for helping me at the moment that I needed it most. Thank you so much! Your orientation made the two years of master's and the four years of doctorate easier. I would also like to thank Professor Dr. Adriana Nunes Correia for all the orientation, advice, and knowledge given to me.

To contribute realized by the Professor Dr. Pierre Basílio Almeida Fechine, Professor Dr. Paulo Naftali Casciano, and Professor Dr. Antoninho Valentini for all contributions in the qualification exam.

To contribute, realized by Professor Dr. Norberto de Kássio Vieira Monteiro, Professor Dr. Adriana Nunes Correia, Professor Dr. Pierre Basílio Almeida Fechine, Professor Dr. Ámison Rick Lopes da Silva, and Professor Dr. Simone Barreira Morais for all their contributions in this thesis.

I also thank all future readers of my work. I have a message for you. If someone says you cannot achieve a certain goal, ignore it and move on. These people do not know your true potential. I believe in you.

This study was financed in part by the Coordenação de Aperfeiçoamento de Pessoal de Nível Superior – Brasil (CAPES) - Finance Code 001.

“I don't know what it's like to give up. With a thousand reasons to cry, I will still choose to smile. I'm still here, I haven't surrendered yet. I have a dream, and I won't stop until I achieve it”.

(Author unknown)

RESUMO

A alta emissão dos gases do efeito estufa (GHGs) na atmosfera, especialmente o gás CO_2, está ocasionando no avanço do aquecimento global, resultando em diversos problemas para a sociedade, como secas, furacões, ondas de calor e inundações. Portanto, é urgente capturar esse gás. Nessa tese, o primeiro trabalho analisou o efeito do aumento da temperatura na absorção de CO_2 usando um solvente eutético profundo (DES) baseado em ureia e cloreto de colina (relina) através das simulações por dinâmica molecular (MD) e interações não covalentes (NCI). Posteriormente, o segundo trabalho analisou o efeito sinérgico de três DESs (etalina, relina e glicelina) e uma nanopartícula de prata (AgNP) no processo de captura de CO_2 através das simulações de MD. No primeiro trabalho, foi observado que o efeito do aumento da temperatura ocasionou na redução do número de ligações de hidrogênio entre as moléculas de CO_2 e de ureia, resultando em valores maiores de energia potencial de interação (IPE) total, indicando que o processo de absorção de CO_2 é mais indicado na temperatura de 303 K, com valor de IPE médio de -3872.54 kJ mol^{-1}. Por outro lado, os resultados de NCI indicaram que o efeito do aumento da temperatura resultou no aumento de interações repulsivas e reduziu as interações atrativas nos sistemas simulados. Portanto, ambas abordagens computacionais sugeriram que o processo de absorção de CO_2 é mais indicado na temperatura de 303 K. Em relação ao segundo trabalho, foi observado que a presença da nanopartícula de prata aumentou o número de ligações de hidrogênio entre as moléculas de CO_2 e as moléculas que agem como doadoras da ligação de hidrogênio (HBD), resultando em valores menores de IPE total, indicando um melhor processo de captura de CO_2, especialmente para o sistema AgNP-relina-CO_2, com valor de IPE médio de -757.68 kJ mol^{-1}. A análise de função de distribuição radial (RDF) indicou que o etilenoglicol e a ureia são as espécies chave no processo de captura de CO_2 para os sistemas AgNP-etalina-CO_2 e AgNP-relina-CO_2, respectivamente. Além disso, o AgNP é a espécie chave no processo de captura de CO_2 para o sistema AgNP-glicelina-CO_2.

Palavras-chave: aquecimento global; dióxido de carbono; solvente eutético profundo; nanopartículas de prata; abordagem computacional.

ABSTRACT

The high levels of greenhouse gas (GHG) emissions in the atmosphere, especially CO_2, are driving global warming, which is causing several problems for society, such as droughts, hurricanes, heat waves, and floods. Therefore, it is urgent to capture CO_2 gas. In this thesis, the first work analyzed the effect of increased temperature on CO_2 absorption using a deep eutectic solvent (DES) based on urea and choline chloride (reline) through molecular dynamics (MD) simulations and non-covalent interactions (NCI). Posteriorly, the second work analyzed the synergistic effect of three DESs (ethaline, reline, and glyceline) and a silver nanoparticle (AgNP) in the CO_2 capture process through MD simulations. In the first work, it was observed that the increased temperature effect occasioned the reduction of the hydrogen bond (HB) number between the CO_2 molecules and the urea molecules, resulting in the highest total interaction potential energy (IPE), indicating that the CO_2 absorption process is more indicated at 303 K, with an average IPE value of -3872.54 kJ mol^{-1}. On the other hand, the NCI results indicated that the increased temperature effect resulted in increased repulsion interactions and reduced the strong interactions in the systems simulated. Therefore, both computational approaches suggested that the CO_2 absorption process is more indicated at the temperature of 303 K. In the second work, it was registered that the AgNP presence increases the HB number between the CO_2 gas and the molecules that act as hydrogen bond donors (HBD), resulting in the lowest total IPE values for this group, occasioning a better CO_2 capture process, especially for the AgNP-reline-CO_2 system, with an average IPE value of -757.68 kJ mol^{-1}. The radial distribution function (RDF) analysis indicated that ethylene glycol and urea are key species in the CO_2 capture process for the AgNP-ethaline-CO_2 and AgNP-reline-CO_2 systems, respectively. Furthermore, the AgNP is the key species in the CO_2 capture process for the AgNP-glyceline-CO_2 system.

Keywords: global warming; carbon dioxide; deep eutectic solvent; silver nanoparticles; computational approach.

LIST OF FIGURES

LIST OF FIGURES – SUPPLEMENTARY MATERIAL

LIST OF TABLES

LIST OF TABLES – SUPPLEMENTARY MATERIAL

LIST OF ABBREVIATIONS AND ACRONYMS

AgNP	Silver nanoparticle
AuNP	Gold nanoparticle
B3LYP	Becke-3-parameter Lee-Yang-Parr
CCN	Cumulative Coordination Number
CCS	Carbon Capture and Storage
CeNPs	Cerium oxide nanoparticles
CFCs	Chlorofluorocarbons
Ch^+	Choline
CH_4	Methane
CHARMM	Chemistry at Harvard Macromolecular Mechanics
CHELPG	CHarges from ELectrostatic Potentials using a Grid-based method
CO_2	Carbon dioxide
Co_3O_4	Cobalt oxide nanoparticles
DESs	Deep Eutectic Solvents
DFT	Density Functional of Theory
E	Ethylene glycol
ECR	Electrochemical CO_2 Reduction
G	Glycerol
GHGs	GreenHouse Gas
GROMACS	Groningen Machine for Chemical Simulation
HB	Hydrogen Bond
HBD	Hydrogen Bond Donor
IPE	Interaction Potential Energy
MD	Molecular Dynamics
MNPs	Metal nanoparticles
NCI	Non-Covalent Interactions
NPT	Constant number of particles, pressure, and temperature
NVT	Constant number of particles, volume, and temperature
OPLS-AA	Optimized Potential for Liquid Simulations – All Atom
RDF	Radial Distribution Function
RDG	Reduced Density Gradient

SDF	Spatial Distribution Function
U	Urea
V_{elec}	Electrostatic contributions
VMD	Visual Molecular Dynamics
V_{vdw}	van der Waals contributions

SUMMARY

1. INTRODUCTION

Global warming is causing the average temperature increase on the surface of the earth because of the high emission of Greenhouse Gases (GHGs) in the atmosphere (VENKATARAMANAN; SMITHA, 2011). This phenomenon has increased extreme weather events, such as droughts, hurricanes, heat waves, and floods (NAVAS-MARTÍN *et al*., 2024), resulting in several problems for society. It was estimated that these extreme events have cost around US$ 143 billion per year due to climatic change (NEWMAN; NOY, 2023). In an attempt to slow the advance of global warming, 196 countries signed the Paris Climate Agreement, which aims to keep global average temperature increases below 2 ºC by reducing GHG emissions into the atmosphere.

The GHGs previously cited are composed of carbon dioxide (CO_2), methane (CH_4), water vapor (H_2O), ozone (O_3), chlorofluorocarbons (CFCs), and nitrous oxide (N_2O) (VENKATARAMANAN; SMITHA, 2011). Among GHGs, CO_2 is the main contributor to global warming (MJALLI *et al*., 2017). The main contributors to high CO_2 emissions were China, the USA, and India (JONES *et al*., 2023), with concentrations of 1.62, 0.71, and 0.35 ppm, respectively (GREENMATCH, 2025). Besides, the CO_2 global concentration in the atmosphere reached a value of 428.62 ppm in January 2026 (NATIONAL OCEANIC AND ATMOSPHERIC ADMINISTRATION – NOAA, 2025), registered by the Mauna Loa Observatory. This value observed is well above the acceptable limit of 350 ppm (MJALLI *et al*., 2017). Therefore, to slow the advance of global warming, it is urgent to develop or improve methods for capturing CO_2.

Carbon Capture and Storage (CCS) employs several methods for CO_2 capture and release from the industrial sector and various other energy sources (YAASHIKAA *et al*., 2019), including combustion, photochemical, biochemical, and electrochemical processes. The combustion process is classified into pre-combustion (YAASHIKAA *et al*., 2019), oxyfuel combustion (MUSKALA *et al*., 2011), post-combustion (KRZYWANSKI *et al*., 2018), and chemical looping combustion (ZYLKA *et al*., 2019). Among these processes, post-combustion is more indicated due to the ease of separating CO_2 gas after combustion and the intuitive retrofitting of existing CO_2 sources (DUTCHER; FAN; RUSSELL, 2015). This process may be realized through cryogenic separation (HE *et al*., 2025), membrane separation (MICARI; DAKHCHOUNE; AGRAWAL, 2021), absorption using solvents (KUSSAINOVA; SHAH, 2020), and adsorption with sorbents (BALASUBRAMANIAM *et al*., 2024). The absorption

technology is more indicated because it can be efficiently applied in plants, such as in the post-combustion process (DUTCHER; FAN; RUSSELL, 2015).

Generally, Ionic Liquids (ILs) and Deep Eutectic Solvents (DESs) are employed in the CO_2 absorption process due to their high affinity with the CO_2 molecules (KUSSAINOVA; SHAH, 2020; NAWAZ KHAN *et al*., 2024). Both solvents have similar physical properties, such as low vapor pressure, relatively wide liquid range, and nonflammability (SMITH; ABBOTT; RYDER, 2014). However, ILs are more expensive than DESs. Besides, this solvent has several advantages over traditional ILs, such as easy preparation and greater chemical inertness.

Some researchers have studied CO_2 capture using the DESs. Ji *et al.* (JI *et al*., 2014) analyzed the CO_2 capture using DESs based on choline chloride and urea through an experimental approach. This work showed that this solvent has a higher CO_2 absorption capacity compared to conventional amine solvents. Furthermore, Kussainova & Shah (KUSSAINOVA; SHAH, 2020) analyzed CO_2 absorption in DESs containing triphenylphosphonium bromide (MTPPBr) and monoethanolamine (MEA) using molecular dynamics (MD) simulations. This work reported strong interactions between MEA/CO_2 and Bromide/CO_2, indicating that MEA and bromide are key components in CO_2 capture.

Another method used in CO_2 capture is Electrochemical CO_2 Reduction (ECR). This method forms important products such as carbon monoxide, formate/formic acid, oxalate/oxalic acid, methanol, methane, formaldehyde, ethanol, and ethylene (YAASHIKAA *et al*., 2019). The main advantages of ECR are that the controlled reaction occurs aided by the electrode potentials and temperature, and the ECR system is easy, modular, and compact for application on a large scale. Besides, recycling electrolytes is possible, resulting in minimized consumption of chemicals (YAASHIKAA *et al*., 2019). Generally, oxides, metal nanoparticles (MNPs), and bimetallic catalysts are used in the ECR method. Among these species, MNPs have received attention as a promising candidate for the ECR method. Furthermore, MNPs exhibit interesting properties, including high activity, stability, and recyclability (YAASHIKAA *et al*., 2019).

Some researchers have used silver (AgNPs) and gold nanoparticles (AuNPs) in the ECR process. Chang *et al.* (CHANG *et al*., 2020) investigated the validity of applying space confinement to increase the faradaic efficiency of the CO_2RR to CO using AgNPs and AuNPs via quantum mechanics calculations. For large-scale ECR processes, the employed Au metal is not favorable due to their high price (NGUYEN *et al*., 2021).

However, the Ag metal may be used instead of Au metal because silver metal is more abundant, has a lower price (compared to Au metal), and has an excellent activity for ECR to CO production (NGUYEN *et al*., 2021). In addition to the reasons above, the AgNP has several applications, including as a photocatalyst (Kang *et al*., 2019), an antibacterial agent (LÓPEZ-CARBALLO *et al*., 2013), and an electronic device (CHUN *et al*., 2009).

To further improve CO_2 capture, some researchers have analyzed the synergistic effect of DESs and MNPs. Ahmad *et al.* (AHMAD *et al*., 2023) analyzed the synergistic effect of DESs (tetrabutylphosphonium bromide and formic acid) and cerium oxide nanoparticles (CeNPs) for CO_2 capture. Furthermore, Noorani *et al.* (NOORANI *et al*., 2023) reported a synergistic effect between cobalt oxide nanoparticles (Co_3O_4 NPs) and DESs (ethylene glycol and choline chloride) for CO_2 capture. Both works reported the synergic effect of CO_2 capture.

Researchers have used a computational approach to understand, at the molecular level, the interactions between CO_2 molecules and the components of the system (BEZERRA *et al*., 2024; KUSSAINOVA; SHAH, 2020). This approach is classified into simulations based on quantum mechanics and molecular mechanics methods. MD simulations based on molecular mechanics were employed in the two chapters of this PhD thesis. On the other hand, the Non-Covalent Interactions (NCI) based on quantum mechanics were utilized only in chapter one.

This PhD thesis reported on the CO_2 capture process using DESs and AgNPs via a computational approach. This PhD thesis was divided into two chapters. Chapter one analyzed the temperature increase in the CO_2 absorption using the DESs based on choline chloride and urea through MD and Non-Covalent Interactions (NCI) simulations. On the other hand, chapter two reported the synergistic effect of AgNPs with ethaline (1ChCl:2E), reline (1ChCl:2U), or glyceline (1ChCl:2G) in the CO_2 capture process via MD simulations. All these systems were simulated and analyzed from September 2022 to December 2025.

Chapter 1

ANALYSIS OF TEMPERATURE IN THE CO_2 ABSORPTION USING A DEEP EUTECTIC SOLVENT: AN *IN SILICO* APPROACH

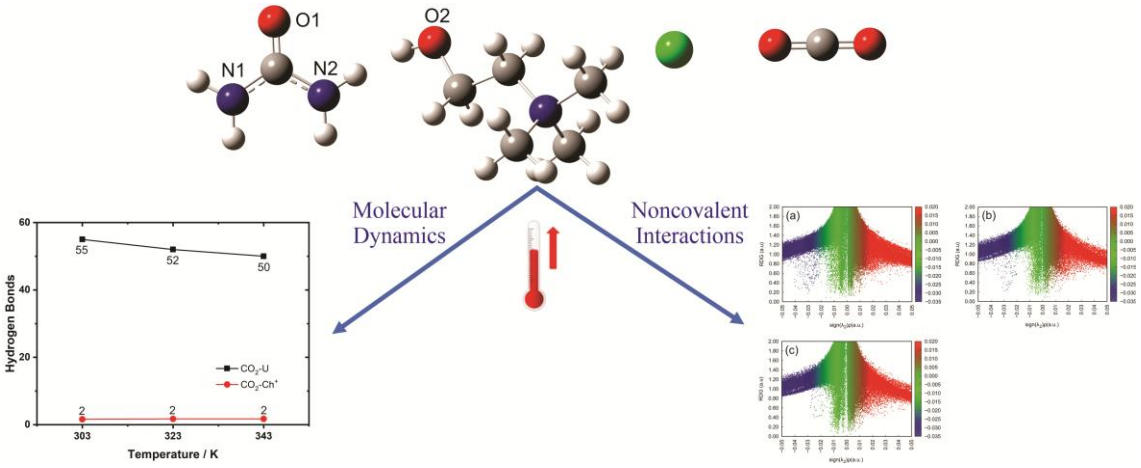

https://doi.org/10.1016/j.jmgm.2023.108649

RESUMO

O excesso de gás carbônico na atmosfera tem contribuído consideravelmente para o aquecimento global, ocasionando diversos danos ao planeta. Portanto, é urgente encontrar formas de capturar esse gás. Então, o presente trabalho analisou o efeito da temperatura na absorção de CO_2 através dos solventes eutético profundos (DESs) baseado em ureia e cloreto de colina utilizando uma abordagem *in silico*. As simulações por dinâmica molecular (DM) indicaram que o aumento da temperatura reduziu o potencial de interação das moléculas de dióxido de carbono com os componentes do DESs, indicando que o processo de absorção é mais indicado em 303 K. Por outro lado, as simulações de interações não covalentes (NCI) sugerem que o aumento da temperatura reduziu as fortes atrações e aumentou as interações repulsivas entre as moléculas de CO_2 com a relina. Portanto, ambas abordagens *in silico* sugerem que a absorção de dióxido de carbono é mais indicada na temperatura de 303 K.

Palavras-chave: aquecimento global; dióxido de carbono; absorção; solvente eutético profundo; abordagem *in silico*.

ABSTRACT

The excess level of carbon dioxide in the atmosphere has contributed a lot to global warming, causing several damages to the planet. Therefore, it is urgent to find ways to capture this gas. Then, the present work analyzed the temperature effect in CO_2 absorption through deep eutectic solvents (DESs) based on urea and choline chloride using an in silico approach. The Molecular Dynamics (MD) simulations indicated that the increased temperature reduced the interaction potential of carbon dioxide molecules with the DESs components, indicating that the absorption process is more indicated at 303 K. On the other hand, the Noncovalent Interactions (NCI) simulations suggest that the increased temperature reduced the strong attractions and increased repulsive interactions between the carbon dioxide molecules with the solvent analyzed. Therefore, both in silico approaches suggest that the carbon dioxide absorption is more indicated at 303 K.

Keywords: global warming; carbon dioxide; absorption; deep eutectic solvents; in silico approach.

1. Objective

1.1 General

- Analyze the effect of increased temperature on CO_2 absorption using DESs based on choline chloride and urea through a computational approach.

1.2 Specifics

- Calculate the hydrogen bond number for the CO_2-U and CO_2-Ch^+ groups as a function of temperature.
- Measure the interaction potential energy between CO_2 molecules and the DESs components.
- Verify the key species in the CO_2 absorption process.
- Analyze the CO_2 solvation layer.
- Obtain the reduced density gradient versus ($\lambda_2\rho$) at different temperatures.

2. Computational details

2.1 Obtain of tridimensional structures and of partial charges

The Density Theory of Functional (DFT) was employed the obtain tridimensional structures (urea, choline, and CO_2) optimized in the gas phase using the hybrid functional B3LYP (PERDEW; BURKE; ERMZERHOF, 1996) with the 6-311+G(d,p) basis set (FRISCH; POPLE; BINKLEY; 1984), implemented in the Gaussian 09 *software* (FRISCH *et al*., 2009). All the frequencies were checked, and the absence of negative vibrational frequencies was constated (Figs. S1, S2, S3 in the supplementary material). Posteriorly, the Multiwfn *software* (LU; CHEN, 2012) was used to obtain the partial charges of urea, choline, and CO_2 species (Table S1, S2, and S3 in the supplementary material, respectively) utilizing the CHELPG method (GARCIA; ATILHAN; APARICIO; 2015). Furthermore, the species in Fig. 1 were employed in the MD simulations.

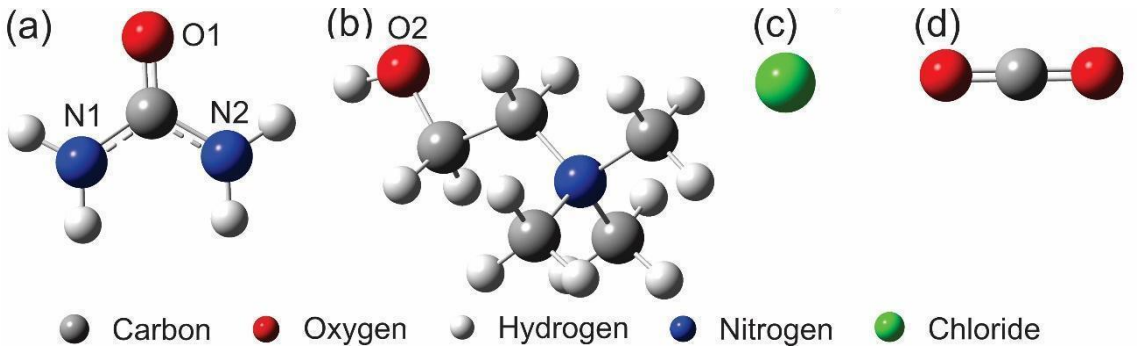

Fig. 1. Tridimensional structures employed in the MD simulations with the nomenclature of main atoms. (a) urea, (b) choline, (c) chloride, and (d) CO_2.

2.2 Molecular dynamics

All the MD simulations were performed using the Gromacs *software* (ABRAHAM *et al*., 2015) version 2021.4 implemented with the OPLS-AA force field (JORGENSEN; TIRADO-RIVES, 1988). First, the CO_2 parameters were taken from Moosavi et al. (MOOSAVI; ABDOLLAHI; RAZMKHAH, 2015). Then, the 56 CO_2 (corresponding to the maximum solubility of CO_2 as observed experimentally in the Leron et al. (LERON; CAPARANGA; LI, 2013), 1160 urea, 580 choline, and 580 chloride species were added in a cubic box of simulation of initial dimensions of 12 × 12 × 12 nm^3 and simulated at 303, 313, 323, 333, and 343 K. A low-density box reaches

faster a better equilibrium and mixture (SHAH; GAPEYENKO; URAKPAYEV; TORKMAHALLEH, 2019; KUSSAINOVA; SHAH, 2020).

The geometry of the system was realized using the steepest descent (HAUG; ARORA; MATSUI, 1976) and gradient conjugate algorithms (YUAN; LI; HU, 2019), both with the energy tolerance of 10 kJ mol^{-1} nm^{-1} and step size of 10^{-1} nm. Posteriorly, the equilibrium dynamics were simulated in 1 ns and divided into two steps. The first step was to apply the ensemble NVT using the Berendsen thermostat (BERENDSEN *et al*., 1984) at 303, 313, 323, 333, and 343 K for respective systems, then, the second step was performed by the ensemble NPT using the Parrinello-Rahman barostat (PARRINELLO; RAHMAN, 1984) with pressure in value of 3.0 bar. Finally, the production step was realized in 100 ns through the Leap-Frog algorithm (GUNSTEREN; BERENDSEN, 1988) using the same temperature and pressure values used in the equilibrium dynamics step. Besides, the production step was simulated in three replicates for each temperature.

The Interaction Potential Energy (IPE) (Equation 1) was calculated by the sum of short-range energies of Lennard-Jones and Coulomb (MANSUROV; SHAH; BAZYBEK; TORKMAHALLEH, 2018) to mensurate the affinity between the CO_2 molecules with the species present in the systems analyzed. The N_i and N_j are the number total of atoms of i and j, respectively. On the other hand, the V_{vdW} and V_{elec} are terms corresponding to the van der Waals forces and electrostatic contributions, respectively.

$$IPE_{i,j} = \sum_{i}^{N_i} V_{vdW}(r_{ij}) + \sum_{j \neq i}^{N_j} V_{elec}(r_{ij}) \quad (1)$$

2.3 Quantum calculations

The equilibrium structures (Fig. 2a) in the last simulation frame (100000 ps) obtained by the MD simulations were chosen as a starting point for the quantum calculations. Only the species within a 4.0 Å radius of the CO_2 molecule (Fig. 2b) were considered for these simulations; this value was employed because the interactions occurred before 4.0 Å among dioxide carbon with the DESs species, as we will see in the RDF results (Fig. 4). Then, the single-point calculations were performed using the ωB97XD (CHAI; HEAD-GORDON, 2008) functional with the 6-311+G(d,p) (FRISCH, M; POPLE, J; BINKLEY, J; 1984) basis set in the Gaussian 09 *software* (FRISCH et al, 2009).

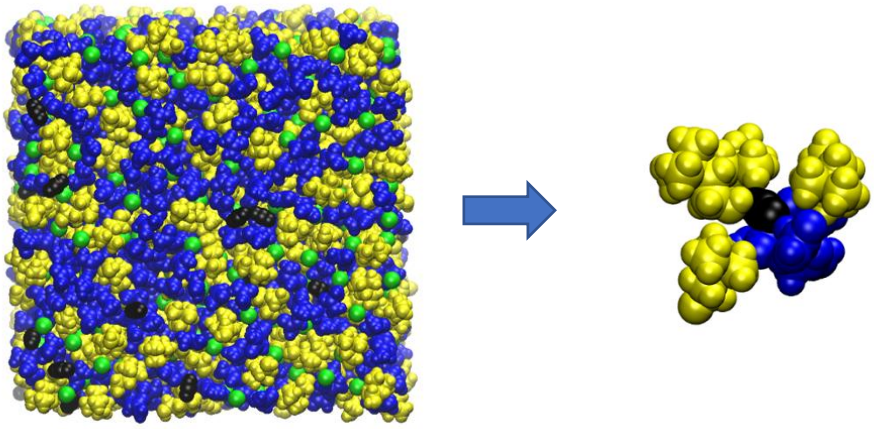

Fig. 2. (a) Snapshot of equilibrium structures in the last simulation frame. (b) Cutting radius of 4.0 Å of species around the CO_2 molecule. The CO_2, urea, choline, and chloride species are represented by the black, blue, yellow, and green colors, respectively.

Posteriorly, the NCI simulations (Equation 2) were realized by the Multiwfn *software* (LU; CHEN, 2012) version 3.8 to analyze noncovalent interactions at the molecular level of single-point calculations. In Equation 2, S is the NCI function, $\nabla\rho(r)$ is the gradient of charge density, and $\rho(r)$ is the electron density. The Reduced Density Gradient (RDG) versus $\lambda_2\,\rho(r)$ distribution shows different noncovalent interactions, like as strong attractive ($\lambda_2\,\rho(r) < 0$) such as hydrogen bonds, van der Waals interactions ($\lambda_2\,\rho(r) \approx 0$), and repulsive interactions ($\lambda_2\,\rho(r) > 0$) such as steric hindrance (JOHNSON; KEINAN; MORI-SÁNCHEZ, 2010).

$$S = \frac{1}{2(3\pi^2)^{\frac{4}{3}}}\frac{|\nabla\rho(r)|}{\rho(r)^{\frac{4}{3}}} \qquad (2)$$

3. Results and discussion

The OPLS parameters utilized to describe the solvent employed in this work were validated by Bezerra et al. (BEZERRA et al, 2022). The validation parameters were realized through specific mass correlation obtained by the experimental and theoretical methods in function of the temperature.

The CO_2 absorption process using the DESs based on urea and choline chloride was analyzed through Hydrogen Bonds (HB), IPE, Radial Distribution Function (RDF), Cumulative Coordination Number (CCN), and NCI results. Fig. 3 shows the average HB number among CO_2 molecules with the Urea (U) and Choline (Ch^+) species in the function of temperature. Furthermore, the HB values for each replicate are registered in Table S4 in the supplementary material. Analyzing this effect, it was observed that the HB number decreased (54.08 to 50.28) between the CO_2 molecules with the U specie. On the other hand, the HB number for the CO_2-Ch^+ group in all the temperatures remained constant. Furthermore, the CO_2-U group registered about 33 times more HB than the CO_2-Ch^+ because the urea molecule has 4 hydrogen bonding sites, while that the choline specie has only one hydrogen bonding site (Fig. S5 in the supplementary material). Therefore, the increased temperature resulted in reduced hydrogen bonds between CO_2 and the DESs studied.

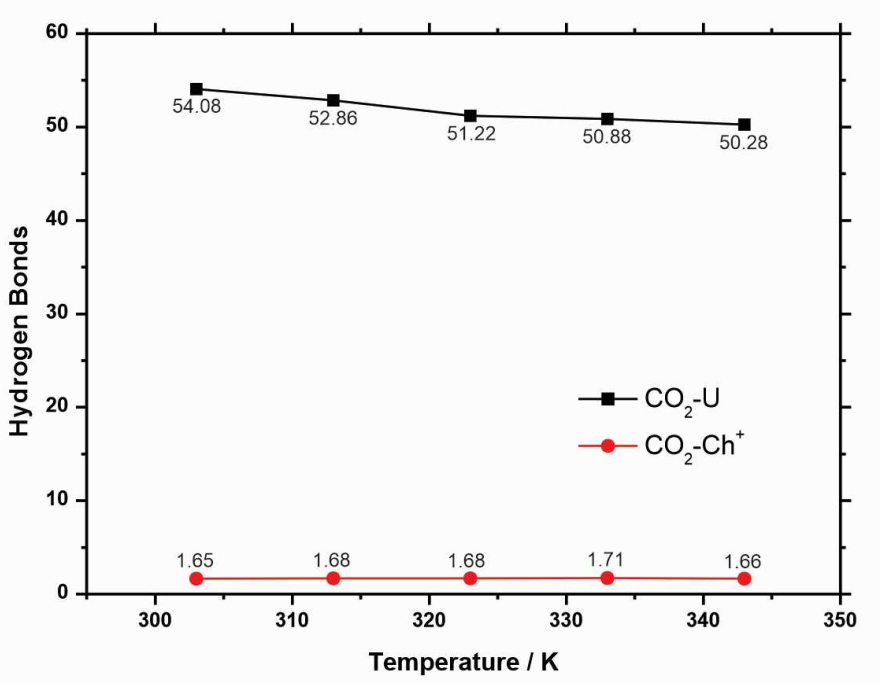

Fig. 3. Number of hydrogen bond between the CO_2-U and CO_2-Ch^+ groups in function of temperature.

Table 1 shows the average IPE values with the standard deviation among the CO_2 molecules with the species in the system. Furthermore, the IPE values for each replicate are registered in Table S5 in the supplementary material. First, it was observed that the CO_2 molecules exhibited a good interaction potential with the U, Ch^+, Cl^- and CO_2 species (independent of temperature analyzed), highlighted for the U and Ch^+ species. The high IPE values registered for the CO_2-U and CO_2-Ch^+ groups are explained by the presence of hydrogen bonds between these species (Figure 3), especially for the CO_2-U group. This intermolecular force may contribute around -1 to -40 kJ mol^{-1} (IZGORODINA; MACFARLANE, 2011) in the interaction potential energy values.

Analyzing this effect, it was observed that occurred an increase in the average IPE values for CO_2-Cl^-, CO_2-U, and CO_2-Ch^+ groups, except for CO_2-CO_2 groups that remained constant. These results indicate that the temperature increase reduced the affinity between CO_2 molecules and species analyzed. Therefore, the CO_2 absorption process in IPE terms is more indicated at 303 K due to the lowest IPE value.

Table 1

Interaction Potential Energy between the CO_2 molecules with the species present in the systems in different temperatures.

Temperature / K	Interaction Potential Energy / kJ mol^{-1}				
	CO_2-CO_2	**CO_2-Cl^-**	**CO_2-U**	**CO_2-Ch^+**	**CO_2-DES**
303	−133.59 (±16.79)	−483.57 (±74.16)	−1959.81 (±141.26)	−1670.72 (±110.71)	−4114.10
313	-134.98 (±18.32)	-479.52 (±78.35)	-1920.54 (±156.07)	-1630.80 (±134.32)	-4030.86
323	−132.09 (±19.30)	−473.52 (±72.58)	−1882.40 (±146.77)	−1610.02 (±123.30)	−3965.94
333	-132.90 (±17.19)	-470.99 (±72.69)	-1865.86 (±158.13)	-1584.02 (±127.39)	-3920.86
343	−131.13 (±19.91)	−461.24 (±75.99)	−1853.08 (±141.90)	−1558.22 (±116.25)	−3872.54

Fig. 4 showed the RDF that realized a structural analysis through the probability density of the species around CO_2 molecules. This analysis is crucial to identify the key species in the absorption process. The CO_2-Cl^- (Fig. 4a), CO_2-U (Fig. 4b), and CO_2-Ch^+

(Fig. 4c) interactions were registered in 3.5 Å, 3.0 Å, and 2.9 Å, respectively. Furthermore, all the species showed similar g(r) values with the CO_2 molecules, indicating that all the solvent components are essential in the absorption process in the RDF terms. Analyzing this effect, it was observed that occurred the reduction of the g(r) values for all interactions. Therefore, the RDF results indicated that the CO_2 absorption process is more indicated at 303 K.

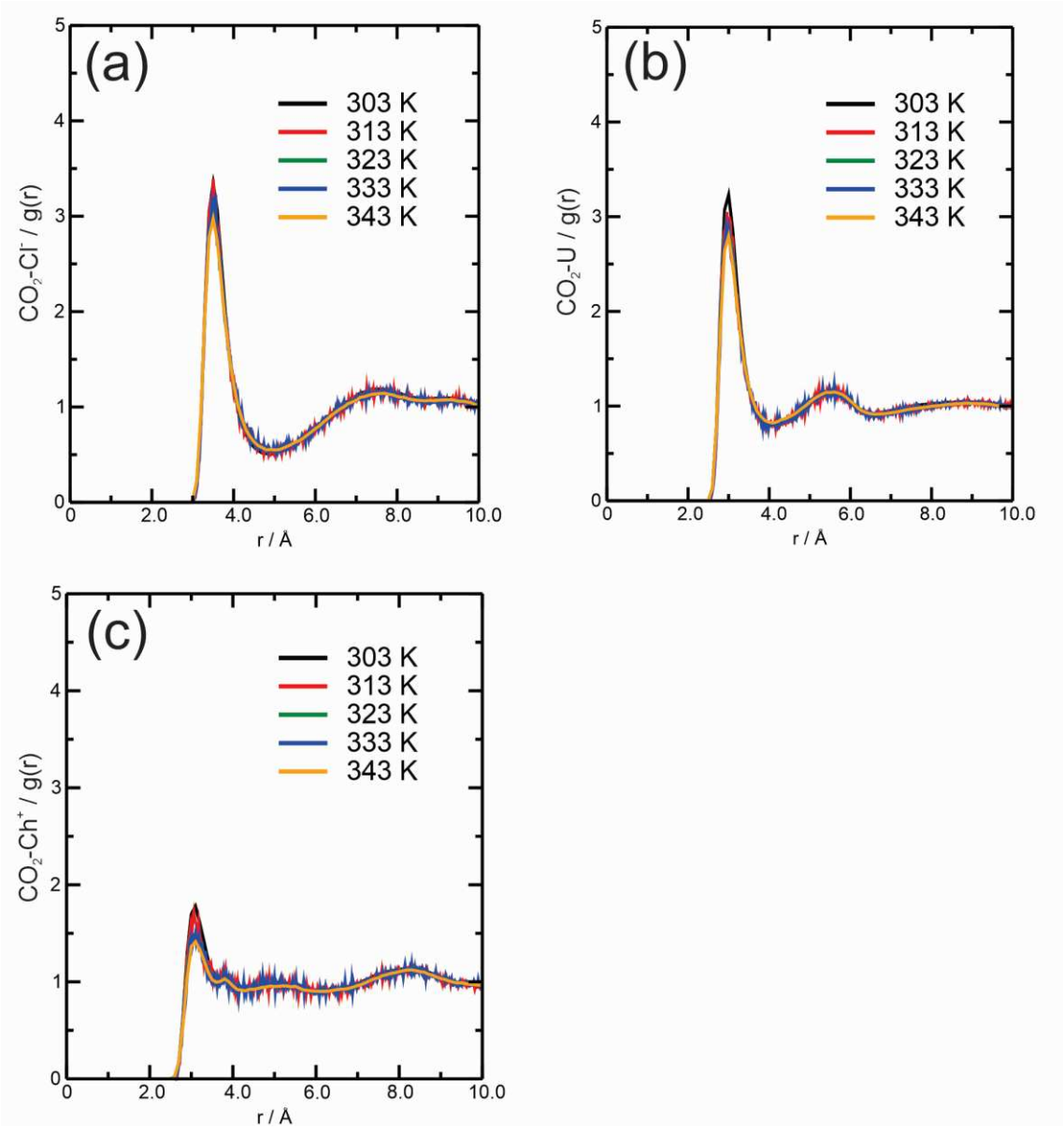

Fig. 4. Radial Distribution Function of (a) CO_2-Cl^-, (b) CO_2-U, and (c) CO_2-Ch^+ interactions in different temperatures.

The CCN analysis (Fig. 5) measures the average species number around the CO_2 molecules. Then, it was observed around 1.0 Cl^- ion (Fig. 5a), 1.5 U molecules (Fig. 5b),

and 0.5 Ch^+ ions (Fig. 5c) around the CO_2 molecules. Furthermore, the CCN results indicated a not well-defined solvation layer. Analyzing this effect, the CCN values did not show significative changes, indicating that the coordination around the CO_2 molecules did not have significative changes. The following analysis will not discuss the systems at the temperature of 313 and 333 K due to the small variation interaction of CO_2 molecules with the solvent analyzed, as observed in the RDF results (Fig. 4) and CCN analysis (Fig. 5).

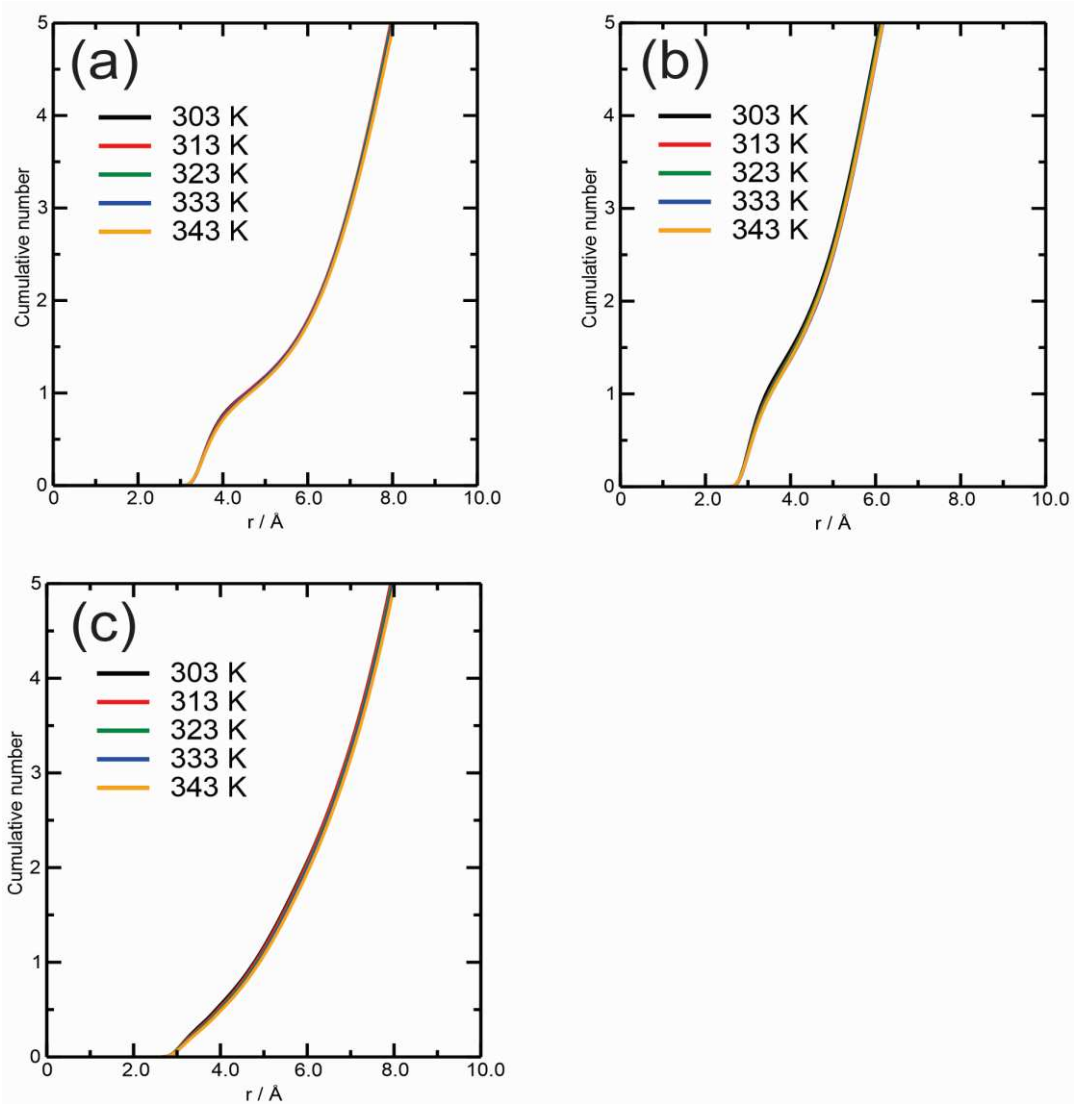

Fig. 5. Cumulative Coordination Number of (a) CO_2-Cl^-, (b) CO_2-U, and (c) CO_2-Ch^+ interactions in different temperatures.

Fig. 6 shows the RDG function versus sign $(\lambda_2)\rho$ for systems at 303, 323, and 343 K. Furthermore, the isovalue employed for this analysis was 0.6, as we may see in Fig. 6. All the RDG graphs showed strong attraction, van der Waals interactions, and strong repulsion. Then, analyzing this effect, a reduction in strong attraction and increased

repulsive interactions among the species present in these systems were observed. Besides, the van der Waals interactions are almost constant with the increased temperature. Therefore, the NCI results suggest that CO_2 absorption is more indicated at 303 K due to many strong interactions and a small number of repulsions. Furthermore, the isosurfaces of RDG function for these systems are present in Fig. S6 in the supplementary material.

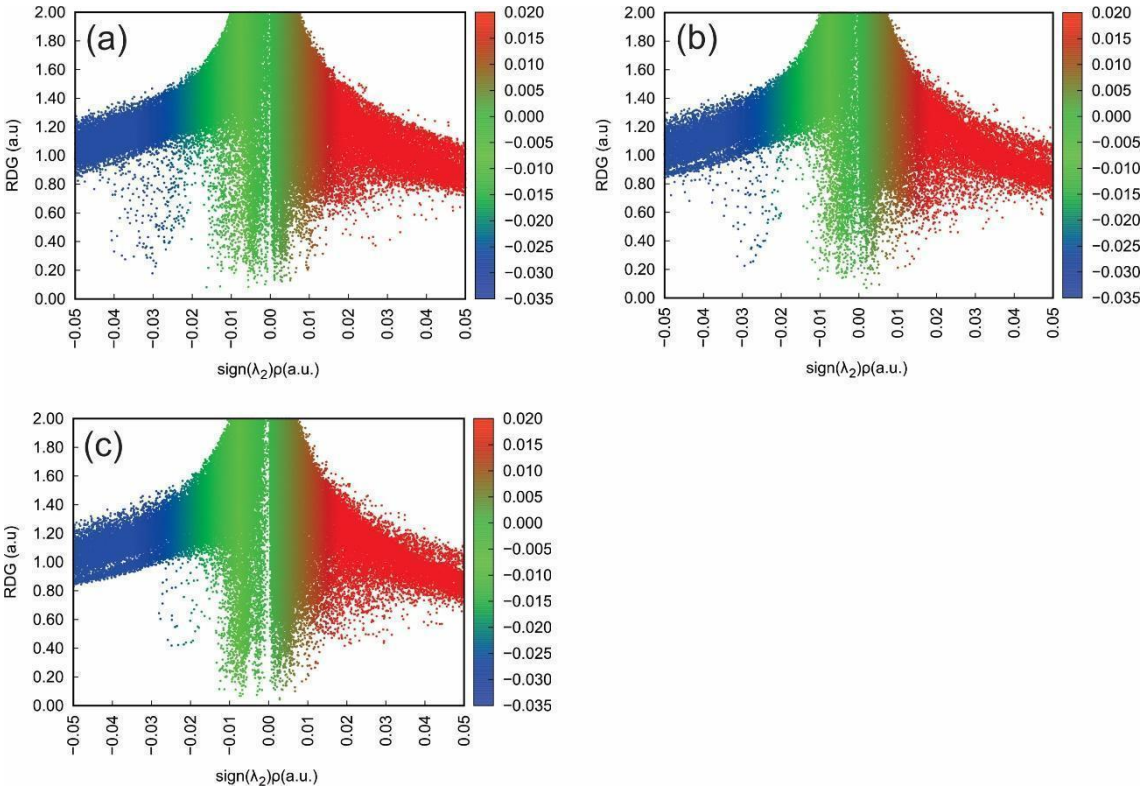

Fig. 6. RDG function versus sign $(\lambda_2)\rho$ plot for the systems at (a) 303, (b) 323, and (c) 343 K.

4. Conclusions

The MD simulations showed that the increased temperature resulted in the reduction of hydrogen bond numbers between CO_2 molecules with the U species, consequently increasing IPE values among CO_2 molecules with the DESs species. Furthermore, this effect reduced the probability density of CO_2 molecules interacting with the DESs species. However, this increased temperature did not affect the solvation layer around the CO_2 molecules. On the other hand, the NCI simulations indicated that the increased temperature reduced strong attractive and increased repulsive interactions between the CO_2 molecules with the DESs species. Therefore, the results indicated that the DES based on urea and choline chloride has higher CO_2 molecules absorption at 303 K.

Supplementary Material

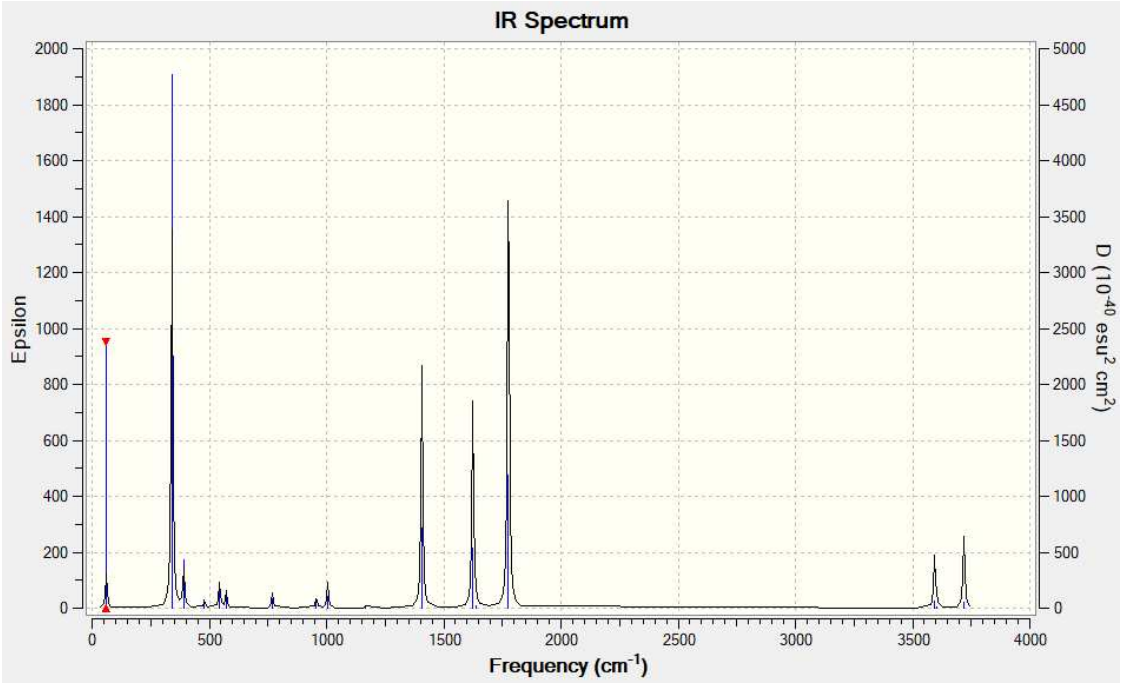

Fig. S1. The vibrational frequencies for the U molecule were calculated by the B3LYP/6-311+G(d,p).

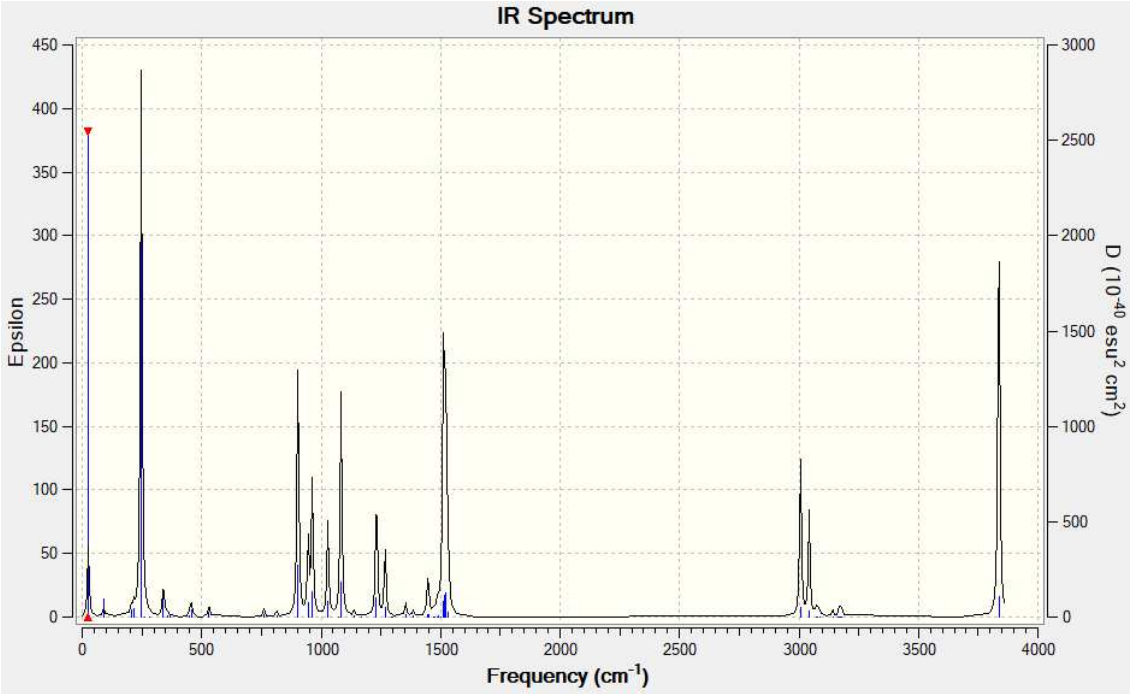

Fig. S2. The vibrational frequencies for the Ch^+ ion were calculated by the B3LYP/6-311+G(d,p).

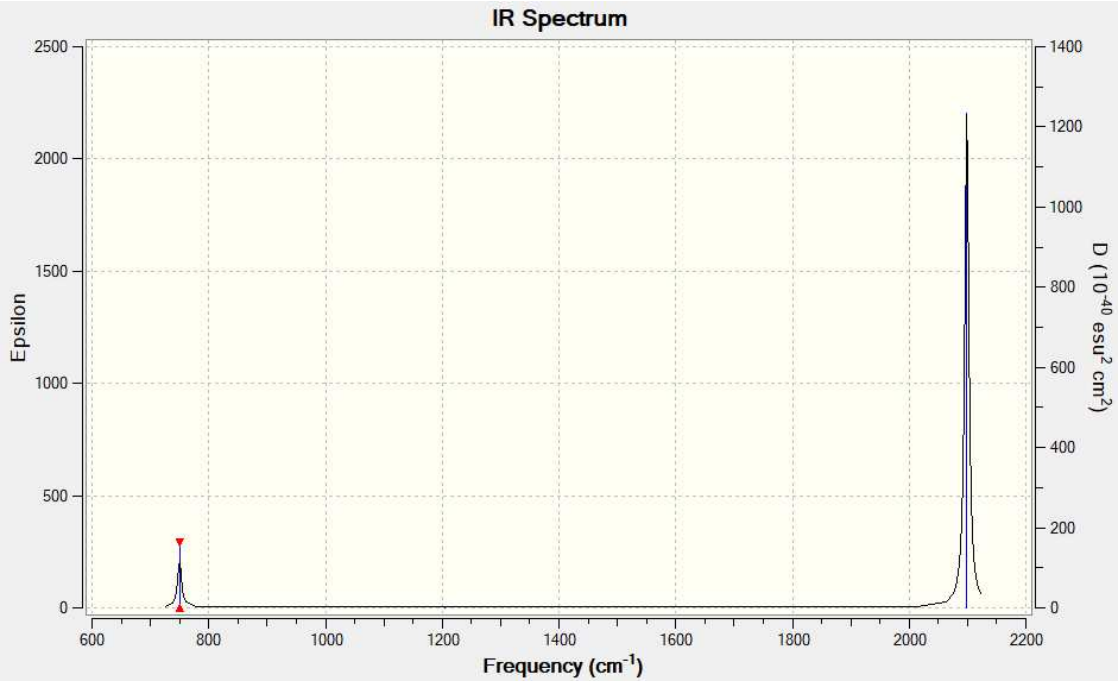

Fig. S3. The vibrational frequencies for the CO_2 molecule were calculated by the B3LYP/6-311+G(d,p).

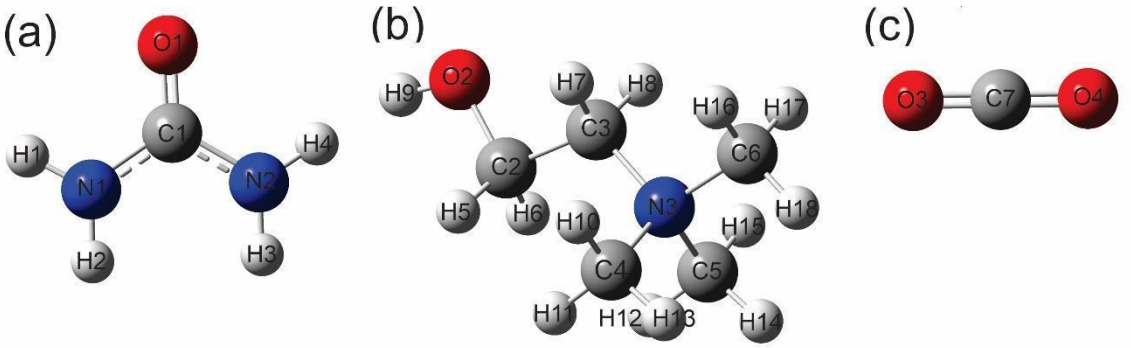

Fig. S4. Nomenclature of all atoms in (a) U, (b) Ch^+, and (c) CO_2 species.

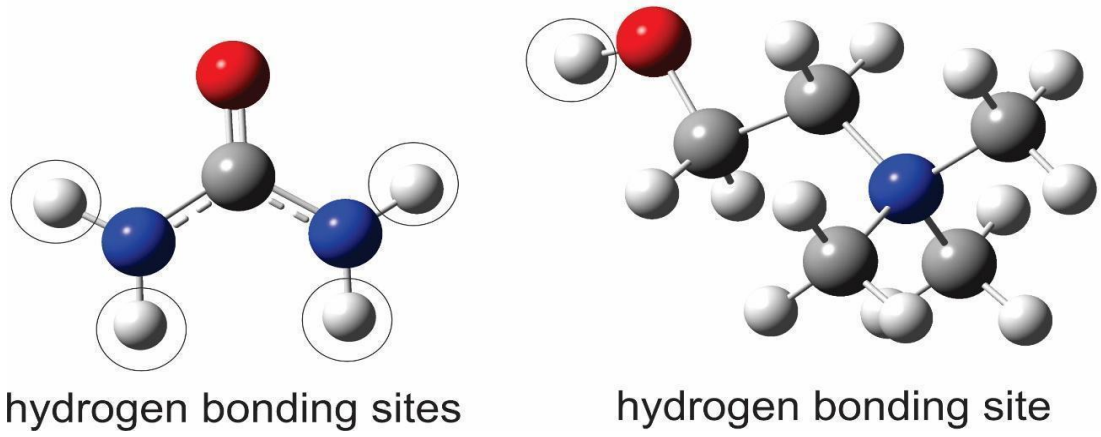

Fig. S5. Hydrogen bonding sites for the U and Ch^+ species.

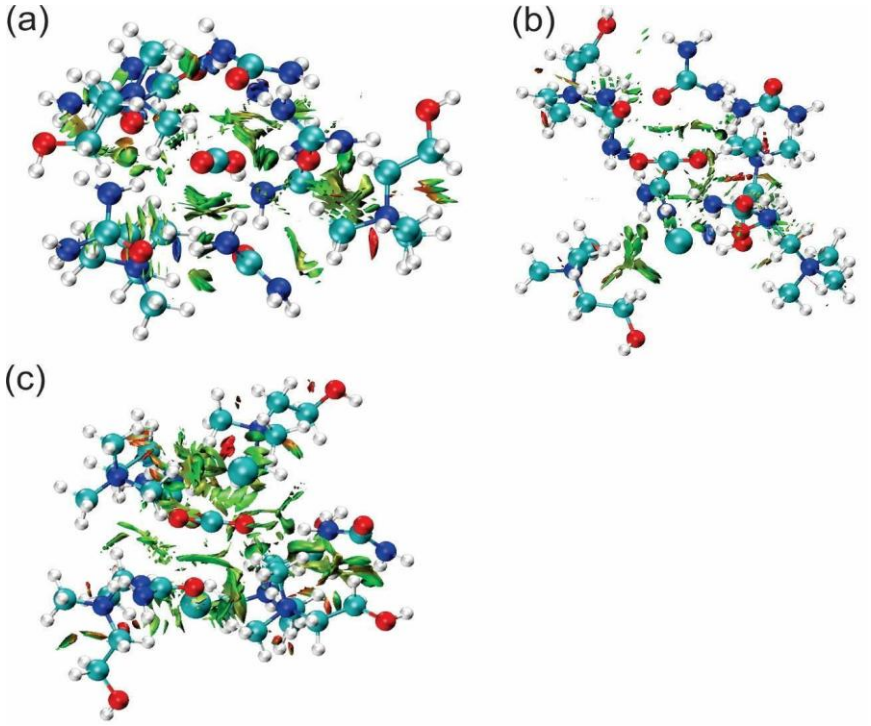

Fig. S6. Isosurfaces of RDG function of systems in the temperatures of (a) 303, (b) 323, and (c) 343 K.

Table S1. Partial charges of U specie.

Atom name	Partial charges (e)
C1	0.884257
N1	−0.839256
N2	−0.837029
O1	−0.620105
H1	0.351016
H2	0.355891
H3	0.350528
H4	0.354698

Table S2. Partial charges of Ch^+ specie.

Atom name	Partial charges (e)
C2	0.018258
H5	0.111847
H6	0.111526
C3	0.287619
H7	0.009572
H8	0.009218
O2	−0.671612
H9	0.454011
N3	0.035607
C4	−0.21053
H10	0.150680
H11	0.150338
H12	0.132613
C5	−0.224576
H13	0.154720
H14	0.136886
H15	0.153094
C6	−0.360751
H16	0.178802
H17	0.178708
H18	0.193973

Table S3. Partial charges of CO_2 specie.

Atom name	Partial charges (e)
C7	1.2082
O3	−0.6041
O4	−0.6041

Table S4. Hydrogen bond values for each replicate between the CO_2 molecules with the U and Ch^+ species in different temperatures.

Temperature / K	Hydrogen bonds		
	Replicate	**CO_2-U**	**CO_2-Ch^+**
303	1	54.59	1.59
	2	53.22	1.79
	3	54.44	1.58
313	1	52.44	1.75
	2	52.65	1.68
	3	53.50	1.62
323	1	51.54	1.70
	2	51.16	1.69
	3	50.96	1.65
333	1	50.38	1.82
	2	51.58	1.69
	3	50.67	1.63
343	1	50.18	1.63
	2	50.45	1.70
	3	50.21	1.64

Table S5. IPE values for each replicate between the CO_2 molecules with the species present in the systems in different temperatures.

Temperature / K	Interaction Potential Energy / kJ mol^{-1}					
	Replicate	**CO_2-CO_2**	**CO_2-Cl^-**	**CO_2-U**	**CO_2-Ch^+**	**CO_2-DES**
303	1	−129.97	−479.17	−1975.27	−1668.73	−4123.17
	2	−136.37	−499.58	−1910.55	−1675.60	−4085.73
	3	−134.43	−471.96	−1993.61	−1667.83	−4133.4
313	1	-128.84	-488.47	-1903.34	-1647.63	-4039.44
	2	-141.05	-466.39	-1950.89	-1613.34	-4030.62
	3	-135.05	-483.69	-1907.38	-1631.44	-4022.51
323	1	−136.67	−467.16	−1882.99	−1624.87	−3975.02
	2	−130.46	−474.11	−1886.57	−1606.79	−3967.47
	3	−129.05	−479.30	−1877.65	−1598.39	−3955.34
333	1	-130.57	-478.96	-1855.02	-1590.48	-3924.46
	2	-133.47	-461.03	-1897.29	-1567.63	-3925.95
	3	-134.67	-472.98	-1845.26	-1593.94	-3912.18
343	1	−133.16	−463.16	−1845.15	−1558.12	−3866.43
	2	−131.67	−453.15	−1864.79	−1554.22	−3872.16
	3	−128.57	−467.41	−1849.30	−1562.33	−3879.04

Chapter 2

SYNERGY EFFECT OF AG NANOPARTICLES AND DEEP EUTECTIC SOLVENTS IN THE CO_2 CAPTURE PROCESS: A COMPUTATIONAL APPROACH

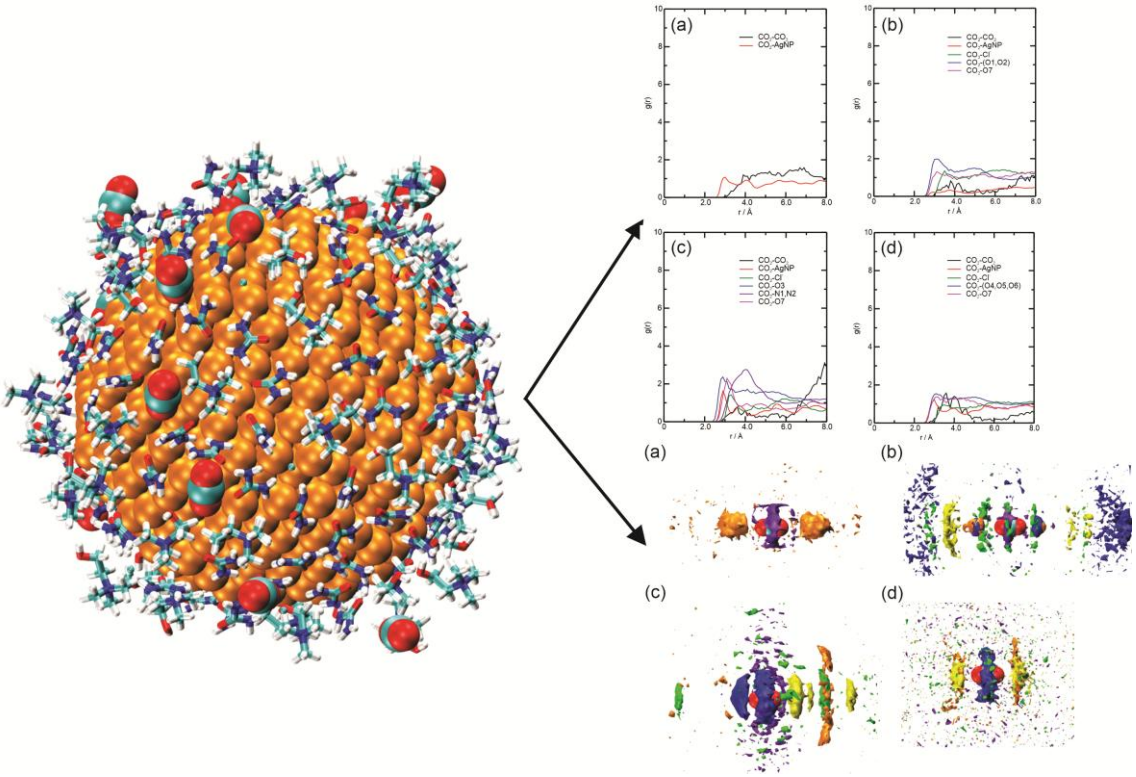

https://doi.org/10.1016/j.molliq.2024.126517

RESUMO

O agravamento do aquecimento global tem ocasionado diversos problemas para o planeta, especialmente devido às altas taxas de emissões de CO_2 na atmosfera. Então, é necessário encontrar novas formas ou aprimorar as já utilizadas na captura do gás CO_2. Esse trabalho analisou através das simulações de dinâmica molecular (DM), o uso de nanopartículas de prata (AgNP) para melhorar a captura de CO_2 nos solventes etalina (1ChCl:2E), relina (1ChCl:2U) e glicelina (1ChCl:2G). As simulações de DM indicaram que a presença de AgNP nos três solventes eutético ocasionaram o aumento do número de ligações de hidrogênio (LH) entre o gás CO_2 e as espécies agindo como doadoras da ligação de hidrogênio (DLH), resultando na redução dos valores da energia potencial de interação para esse grupo, resultando em uma melhora do processo de captura de CO_2, especialmente para o sistema AgNP-relina-CO_2. Além disso, a partir da análise estrutural das simulações da DM é sugerido que o etilenoglicol e a ureia são as espécies chave no processo de captura de CO_2 para os sistemas de AgNP-etalina-CO_2 e AgNP-relina-CO_2, respectivamente. Para o sistema AgNP-glicelina-CO_2, a análise estrutural indicou que a AgNP é a espécie chave no processo de captura de CO_2.

Palavras-chave: Aquecimento global; solvente eutético profundo; nanopartículas de prata; simulações computacionais.

ABSTRACT

The worsening of global warming has caused several problems for the planet, especially due to the high CO_2 emissions in the atmosphere. Then, it is necessary to find new ways or improve the ways already used to capture the CO_2 gas. This work reported through Molecular Dynamics (MD) simulations, the use of silver nanoparticles (AgNP) to improve the CO_2 capture in the ethaline (1ChCl:2E), reline (1ChCl:2U), and glyceline (1ChCl:2G) solvents. The MD simulations indicated that the AgNP presence in the three solvents occasioned increased hydrogen bonds (HB) between the CO_2 gas and species acting as hydrogen bond donors (HBD), resulting in a reduction of interaction potential values for this group, resulting in improvement of CO_2 process capture, especially for the AgNP-reline-CO_2 system. Furthermore, the structural analysis from MD simulations suggested that ethylene glycol and urea are the key species in the CO_2 capture process for the AgNP-ethaline-CO_2 and AgNP-reline-CO_2 systems, respectively. For the AgNP-glyceline-CO_2 system, the structural analysis indicates that the AgNP is the key species in the CO_2 process capture.

Keywords: Global warming; deep eutectic solvents; silver nanoparticles; computational simulations.

1. Objective

1.1 General

- Analyze the synergic effect of AgNP and DESs in the CO_2 capture process through a computational approach.

1.2 Specifics

- Verify in which time interval the DESs-CO_2, AgNP-CO_2, and AgNP-DESs-CO_2 systems reached equilibrium.
- Calculate the hydrogen bond number for the CO_2-HBD and CO_2-Ch^+ groups in the DESs-CO_2 and AgNP-DESs-CO_2 systems.
- Measure the IPE values between the CO_2 molecules and the species present in the DESs-CO_2, AgNP-CO_2, and AgNP-DESs-CO_2 systems.
- Verify the key species in the CO_2 capture process in different systems.

2. Computational details

2.1 Quantum calculations

The ethylene glycol, urea, glycerol, choline, carbon dioxide, and water tridimensional structures were optimized in the gas phase based on the Density Theory Functional (DFT) using the hybrid B3LYP functional (PERDEW; BURKE; ERMZERHOF, 1996) and 6-311+G(d,p) (FRISCH, M; POPLE, J; BINKLEY, J; 1984) basis through Gaussian09 *software* (FRISCH et al, 2009). The optimized structures were checked for the absence of negative frequencies, indicating that species are not in the transition state.

2.2 CHARMM-GUI server

The CHARMM-GUI server (JO; KIM; IYER; IM, 2008) was utilized through the nanomaterial modeler (CHOI et al, 2022) module to obtain the icosahedral AgNP tridimensional structure in the vacuum with a diameter of 1.5 nm (containing 856 silver atoms). Besides, the icosahedral AgNP is most stable with less 1130 silver atoms (AKBARI; MORAD; MAAZA, 2023). The parameters utilized to describe the ethylene glycol, urea, glycerol, choline, carbon dioxide, and water species were obtained by the ligand reader & modeler (KIM et al, 2017) module.

2.3 MD simulations

All the MD simulations were performed by the Gromacs (ABRAHAM *et al*., 2015) *software* implemented with the CHARMM36 force field (LEE et al, 2016). The DESs-CO_2 (ethaline-CO_2, reline-CO_2, glyceline-CO_2), AgNP-CO_2, and AgNP-DESs-CO_2 (AgNP-ethaline-CO_2, AgNP-reline-CO_2, and AgNP-glyceline-CO_2) systems were simulated in a cubic box with initial dimensions of 7 nm × 7 nm × 7 nm. A low-density box reaches the equilibrium faster in the mixture (SHAH; GAPEYENKO, 2019).

For systems with the AgNP, the number of species employed for each system was 1 AgNP, 342 hydrogen bond donors (ethylene glycol, urea, or glycerol), 171 choline ions, 171 chlorides ions, and 15 carbon dioxide (Fig. 1) employed in the MD simulations. Furthermore, the same quantities were utilized for the systems without the AgNP. These quantities are employed based on the CO_2 maximum solubility of 0.2529 mol kg^{-1} on ethaline solvent (LERON; LI, 2013). The same quantity of ethylene glycol was used for the urea and glycerol molecules to compare with the other two solvents. The temperature of 303.15 K and the pressure of 5.37 bar are employed based on the Leron and Li

(LERON; LI, 2013). Fig. 7 shows the tridimensional structures with the nomenclature used for the main species for the RDF analysis (Fig. 11).

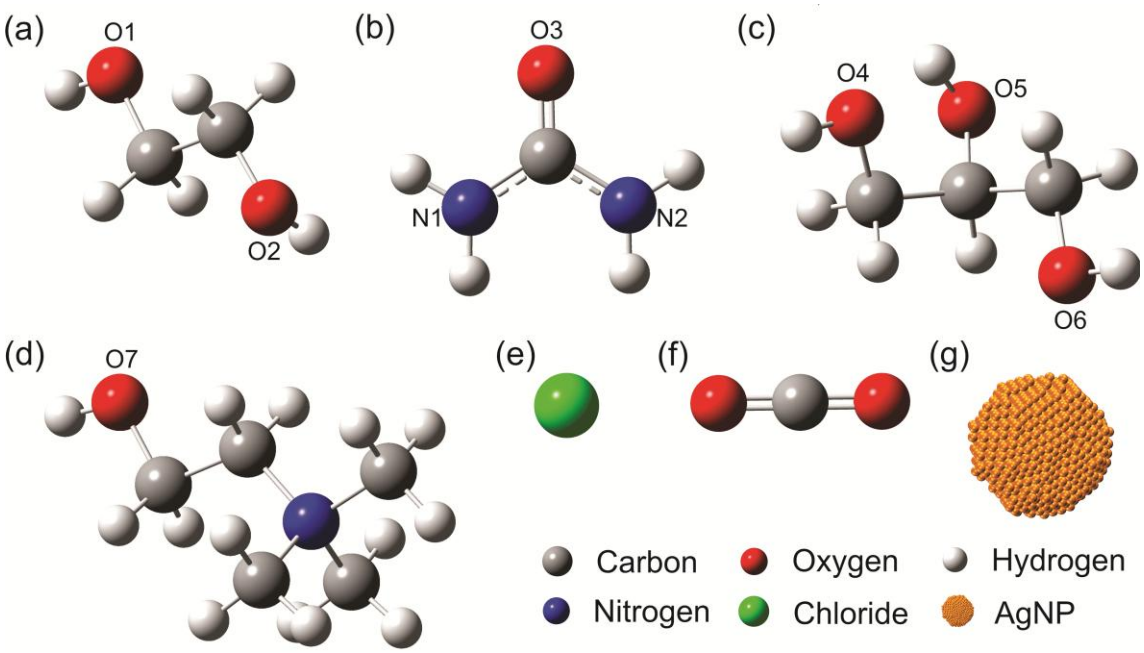

Fig. 7. Tridimensional structures of (a) ethylene glycol, (b) urea, (c) glycerol, (d) choline, (e) chloride, (f) carbon dioxide, (g) AgNP, and (h) water utilized in the MD simulations.

The optimization of the system was performed through steepest descent (HAUG; ARORA; MATSUI, 1976) and gradient conjugate (YUAN; LI; HU, 2019) algorithms, both with an energy tolerance of 100 kJ mol^{-1} nm^{-1}. Posteriorly, the equilibrium dynamics step was simulated initially through the NVT ensemble using the V-rescale (BUSSI; DONADIO; PARRINELLO, 2007) at a temperature of 303.15 K, followed by the NPT ensemble through Parrinello-Rahman (PARRINELLO; RAHMAN, 1984) with a pressure of 5.37 bar. Besides, both ensembles were simulated at 400 ps. Finally, the production step was performed in 100 ns in three replicates.

The Interaction Potential Energy (IPE) (Equation 3) measures the affinity between the CO_2 molecules with the others species. This energy is obtained by the sum of the short-range of van der Waals (V_{vdW}) and electrostatic (V_{elec}) energies (AMORIM-CARMO et al, 2019). The N_i and N_j terms are the number total of atoms of i and j, respectively.

$$IPE_{i,j} = \sum_{i}^{N_i} V_{vdW}(r_{ij}) + \sum_{j \neq i}^{N_j} V_{elec}(r_{ij}) \quad (3)$$

3. Results and discussion

The Root Mean Square Deviation (RMSD) results were used to analyze the equilibrium of systems. Posteriorly, the Hydrogen Bonds (HB) and IPE results were used to analyze the CO_2 capture in the systems simulated. Furthermore, the Radial Function of Distribution (RDF) and Spatial Distribution Function (SDF) the results were used to perform a structural analysis of the systems after CO_2 capture.

The RMSD analysis was performed for the DESs-CO_2 (Fig. 8) and AgNP-DESs-CO_2 (Fig. 9) systems. In this analysis, the system was utilized as a reference to obtain the RMSD results. Furthermore, the black, red, and green line represents each replicate of the systems simulated. The ethaline-CO_2 (Fig. 8a), glyceline-CO_2 (Fig. 8c), AgNP-CO_2 (Fig. 9a), and AgNP-reline-CO_2 (Fig. 9c) systems reached equilibrium around 2 ns. On the other hand, the reline-CO_2 (Fig. 8b) reached equilibrium around 20 ns, while the AgNP-ethaline-CO_2 (Fig. 9b) and AgNP-glyceline-CO_2 (Fig. 9d) reached equilibrium around 60 ns, respectively. The following analysis was based on the trajectories in the last 10 ns. Furthermore, it was also observed that AgNP addition in all the DESs-CO_2 systems significantly decreases the RMSD values, especially for the AgNP-reline-CO_2 system (Fig. 9c), indicating more stable interactions in this system.

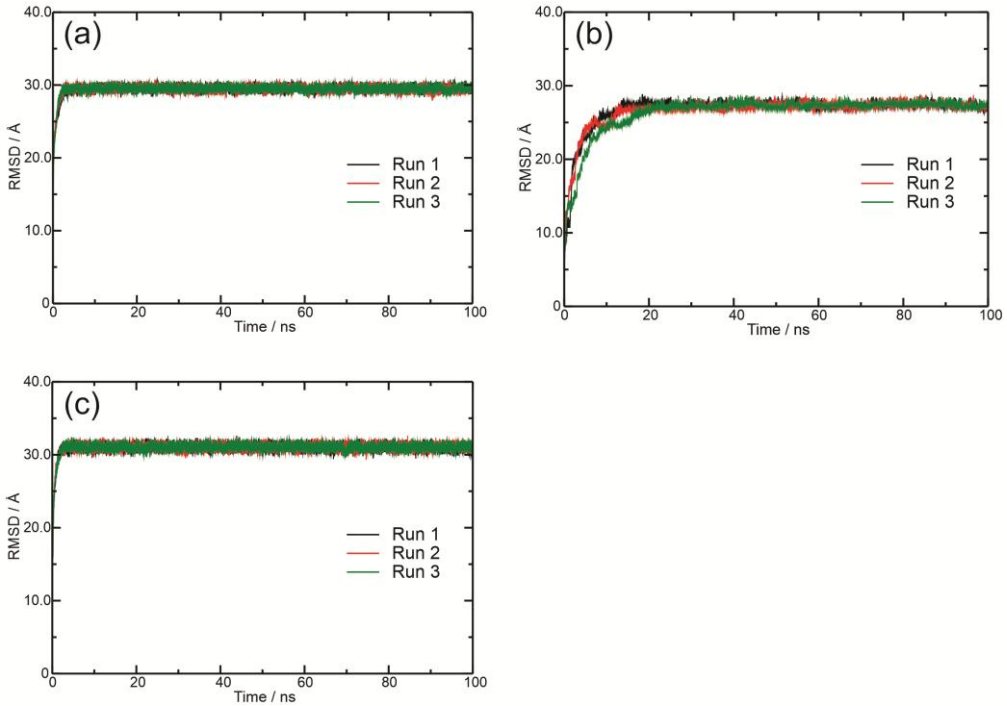

Fig. 8. RMSD of (a) ethaline-CO_2, (b) reline-CO_2, and (c) glyceline-CO_2 systems. The black, red, and green colors represent each replicate simulated.

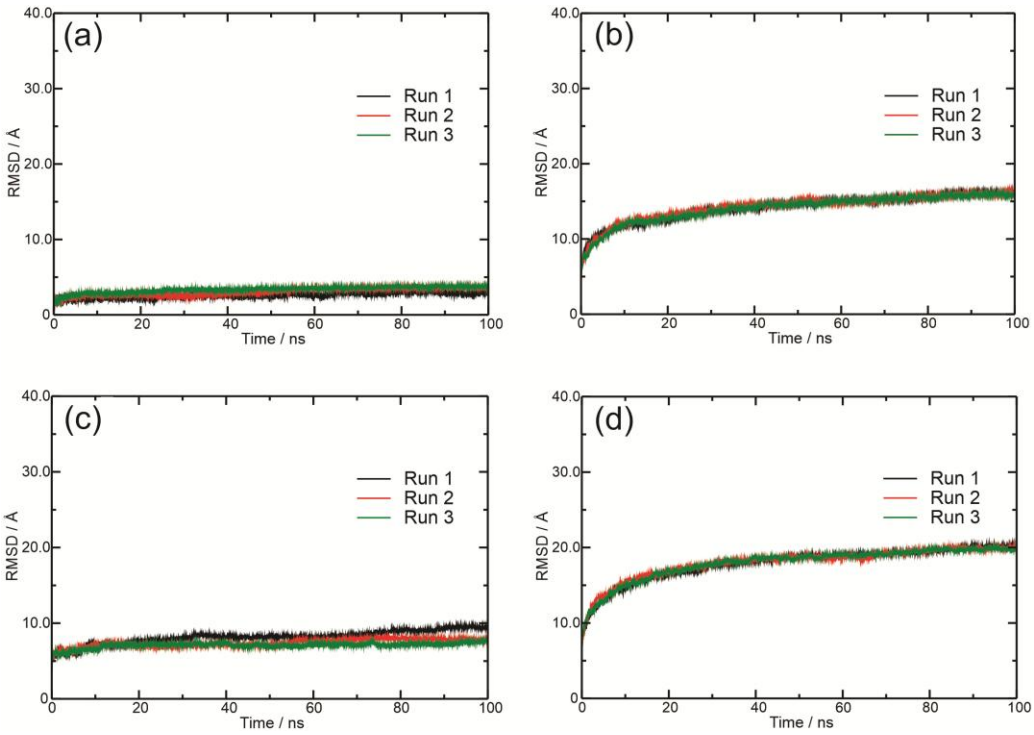

Fig. 9. RMSD (a) AgNP-ethaline-CO_2, (b) AgNP-reline-CO_2, and (c) AgNP-glyceline-CO_2 systems. The black, red, and green colors represent each replicate simulated.

Table 2 shows the average HB of the CO_2-HBD and CO_2-Ch^+ groups for all the systems. The HB values for each replicate are present in the supplementary material (Table S6). It was observed that the reline-CO_2 and AgNP-reline-CO_2 systems registered the highest average HB number at the values of 3.78 and 5.60, respectively. This highest average HB number may be explained because the urea molecules have four hydrogen bond sites (Fig. 10b), while the ethylene glycol and glycerol molecules have two and three hydrogen bond sites (Figs. 10a and 10c), respectively. On the other hand, the CO_2-Ch^+ group registered an average HB number near zero (Table 2) in all the simulated systems. This fact can be explained by the choline ion having only one hydrogen bond site (Fig. 10d). The AgNP presence did not significantly change the HB values for CO_2-Ch^+ interaction. However, an increase in the HB values in AgNP presence was observed for the CO_2-HBD group, especially for the AgNP-reline-CO_2 system. This increase may be explained by the high affinity between the AgNP and urea molecules (Table S7 in the supplementary material). Consequently, some urea species are adsorbed on the AgNP and interact more easily through HB with the CO_2 molecules, which, too, are adsorbed in the AgNP. On the other hand, it was expected that a greater change in HB values for the CO_2-G interaction (of the glyceline-CO_2 concerning the AgNP-glyceline-CO_2) due to the

lowest average IPE values (Table S7 in the supplementary material) between the AgNP and glycerol molecules. However, the glycerol has only three HB sites (as mentioned above), while the urea molecules have four HB sites.

Table 2

Average number of hydrogen bonds between the CO_2-HBD and CO_2-Ch^+ species for the systems analyzed.

Systems	Average hydrogen bonds	
	CO_2-HBD	**CO_2-Ch^+**
ethaline-CO_2	0.67	0.15
reline-CO_2	3.78	0.12
glyceline-CO_2	1.30	0.18
AgNP-ethaline-CO_2	0.89	0.18
AgNP-reline-CO_2	5.60	0.03
AgNP-glyceline-CO_2	1.44	0.14

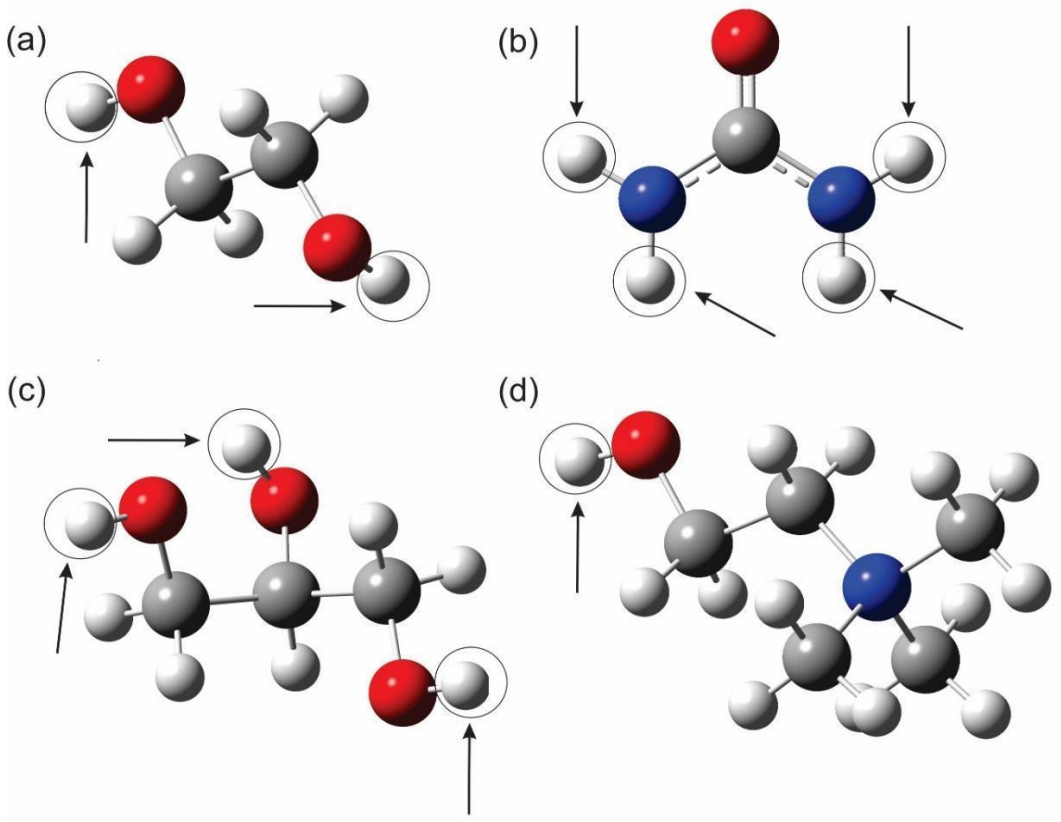

Fig. 10. Hydrogen bond sites for the (a) ethylene glycol, (b) urea, (c) glycerol, and (d) choline species.

The average IPE values are present in Table 3 for all the systems simulated. The supplementary material presents all the IPE values for each replicate (Table S8, S9, and S10). For the systems without the AgNP, the reline-CO_2 system registered the highest total IPE at the value of -542.27 kJ mol^{-1}. This highest total IPE value may be explained by the highest average HB number observed for the CO_2-HBD group in the reline-CO_2 system concerning the same group in the other systems (ethaline-CO_2 and glyceline-CO_2). Furthermore, the HB interaction between these species plays a role in the CO_2 capture process because this intermolecular force may contribute around -1 to -40 kJ mol^{-1} (IZGORODINA; MACFARLANE, 2011) for the IPE value.

For the systems with the AgNP, the AgNP-CO_2 system registered an average IPE value of -1086.73 kJ mol^{-1} between the CO_2 molecules and the AgNP, indicating a strong interaction between them. All contributions to the AgNP-CO_2 interaction energy arise from short-range van der Waals interactions, since the AgNP atoms were modeled with zero partial charges, resulting in a null electrostatic contribution for these specific interactions. On the other hand, analyzing the average IPE value of CO_2-AgNP interaction in the AgNP-ethaline-CO_2 (-248.56 kJ mol^{-1}), AgNP-reline-CO_2 (-235.37 kJ mol^{-1}), and AgNP-glyceline-CO_2 (-220.13 kJ mol^{-1}) systems, it was observed a decrease in affinity for this interaction. This decrease in these systems above may be explained by the CO_2 molecules interacting with other species (Cl^-, HBD, and Ch^+), especially for the HBD species, as seen in Table 2.

For the CO_2-Cl^- interaction, the ethaline-CO_2, reline-CO_2, and glyceline-CO_2 systems registered average IPE values of -15.98 kJ mol^{-1}, -28.97 kJ mol^{-1}, and -11.84 kJ mol^{-1}, respectively. On the other hand, concerning the same interaction, the AgNP-ethaline-CO_2, AgNP-reline-CO_2, and AgNP-glyceline-CO_2 systems registered average IPE values of -21.51 kJ mol^{-1}, -35.44 kJ mol^{-1}, and -16.31 kJ mol^{-1}, respectively. Then, it was observed that the AgNP presence did not significantly change the CO_2 interactions with the Cl^- species. This fact is associated with the lowest IPE values registered between the chloride anion and the AgNP concerning the other interactions (HBD-AgNP and Ch^+-AgNP). These data are presented in Table S7 in the supplementary material. For the CO_2-HBD interaction, it was observed a decrease in the average IPE values of -208.28 kJ mol^{-1} to -230.92 kJ mol^{-1}, -253.95 kJ mol^{-1} to -284.80 kJ mol^{-1}, and -231.21 kJ mol^{-1} to -268.80 kJ mol^{-1} for the AgNP-ethaline-CO_2, AgNP-reline-CO_2, and AgNP-glyceline-CO_2 systems, respectively. This decrease in average IPE values for these systems above suggested an increase in affinity between the CO_2 and HBD species, indicating an

improvement in the CO_2 capture process (concerning this interaction). It was observed a decrease in the average IPE values for the CO_2-Ch^+ interaction of -196.63 kJ mol^{-1} to -213.01 kJ mol^{-1} and -161.77 kJ mol^{-1} to -170.67 kJ mol^{-1} for the AgNP-ethaline-CO_2 and AgNP-glyceline-CO_2 systems, respectively. However, the same interaction showed an increase in the average IPE values of -259.28 kJ mol^{-1} to -202.07 kJ mol^{-1} for the AgNP-reline-CO_2 system, indicating a worse in the CO_2 capture process (concerning this interaction).

The IPE results suggested that the AgNP-CO_2 system has the lowest average total IPE values, indicating that this system has a better CO_2 capture process than the others. However, analyzing this system from an experimental point of view, most nanomaterials will aggregate with each other naturally, causing the limitation of capacity capture of certain compounds (ABO-HAMAD; HAYYAN; ALSAADI; HASHIM, 2015). Then, a DESs may be used as a functionalizing agent to stabilize the AgNP against the aggregation (DAS; KUMAR; RAYAVARAPU, 2021), resulting in better CO_2 capture. Therefore, among the AgNP-DESs-CO_2 systems, the AgNP-reline-CO_2 system has the better CO_2 capture process due to the lowest average total IPE of -757.68 kJ mol^{-1}. The RDF and SDF analysis (Figs. 11 and 12) were realized only for the systems with the AgNP due to the better average IPE values.

Table 3

IPE values between the CO_2 molecules and the species in all the simulated systems.

	Average interaction potential energy / kJ mol^{-1}						
Systems / Interactions	CO_2-CO_2	CO_2-AgNP	CO_2-Cl^-	CO_2-HBD	CO_2-Ch^+	CO_2-DESs	CO_2-DESs-AgNP
ethaline-CO_2	-7.58		-15.98	-208.28	-196.63	-420.88	
reline-CO_2	-8.19		-28.97	-253.95	-259.28	-542.27	
glyceline-CO_2	-7.29		-11.84	-231.21	-161.77	-404.81	
AgNP-CO_2	-12.80	-1086.73					
AgNP-ethaline-CO_2	-5.27	-248.56	-21.51	-230.92	-213.01	-465.44	-714.00
AgNP-reline-CO_2	-7.94	-235.37	-35.44	-284.80	-202.07	-522.31	-757.68
AgNP- glyceline-CO_2	-6.25	-220.13	-16.31	-268.80	-170.67	-455.79	-675.92

The RDF analysis (Fig. 11) represents the probability density of CO_2 species interacting with the other system components in function of radius. This analysis is very important to find the key species in the capture process. The oxygen atom from the CO_2 molecule was used as a reference in the RDF analysis. For the AgNP-CO_2 system (Fig. 11a), the CO_2-AgNP interaction registered a high g(r) value of around 3.0 Å. Concerning the AgNP-ethaline-CO_2 system (Fig. 11b), it was observed that the interaction between the CO_2 molecules and hydrogen atoms (H1,H2) of ethylene glycol species registered the highest g(r) value around 3.8 Å. This high g(r) value is probably associated with the weak hydrogen bonds between the oxygen atom from the CO_2 molecules and the hydrogen atoms (H1,H2) from the ethylene glycol. On the other hand, the other interactions (CO_2-AgNP, CO_2-Cl^-, and CO_2-H10) registered low g(r) values, then, these interactions will not be discussed.

For the AgNP-reline-CO_2 system (Fig. 11c), the main interaction was between the CO_2 molecules and the hydrogen atoms (H3,H4,H5,H6) from the urea around 3.5 Å. This highest g(r) value can be explained by the weak hydrogen bonds between the oxygen atoms from the CO_2 molecule and the hydrogen atoms from the urea molecule. The second interaction most likely to occur was between the CO_2 molecules and the AgNP, this high probability is associated with the highest volume occupied by the AgNP, increasing the probability of CO_2 molecules interacting with the AgNP. The other interactions (CO_2-Cl^- and CO_2-H10) registered the lowest g(r) values and will not be discussed. Concerning the AgNP-glyceline-CO_2 system (Fig. 11d), it was observed that the interactions between CO_2 molecules and the AgNP registered the highest g(r) values. These highest g(r) values are associated with the high volume occupied by the AgNP in the box simulation. The other interactions [CO_2-Cl^-, CO_2-(H7,H8,H9), and CO_2-H10] registered lowest g(r) values, then, will not be discussed. Therefore, the RDF results indicated that the ethylene glycol, urea, and AgNP are the key species in the CO_2 capture process due to the highest g(r) values in the AgNP-ethaline-CO_2, AgNP-reline-CO_2, and AgNP-glyceline-CO_2 systems, respectively.

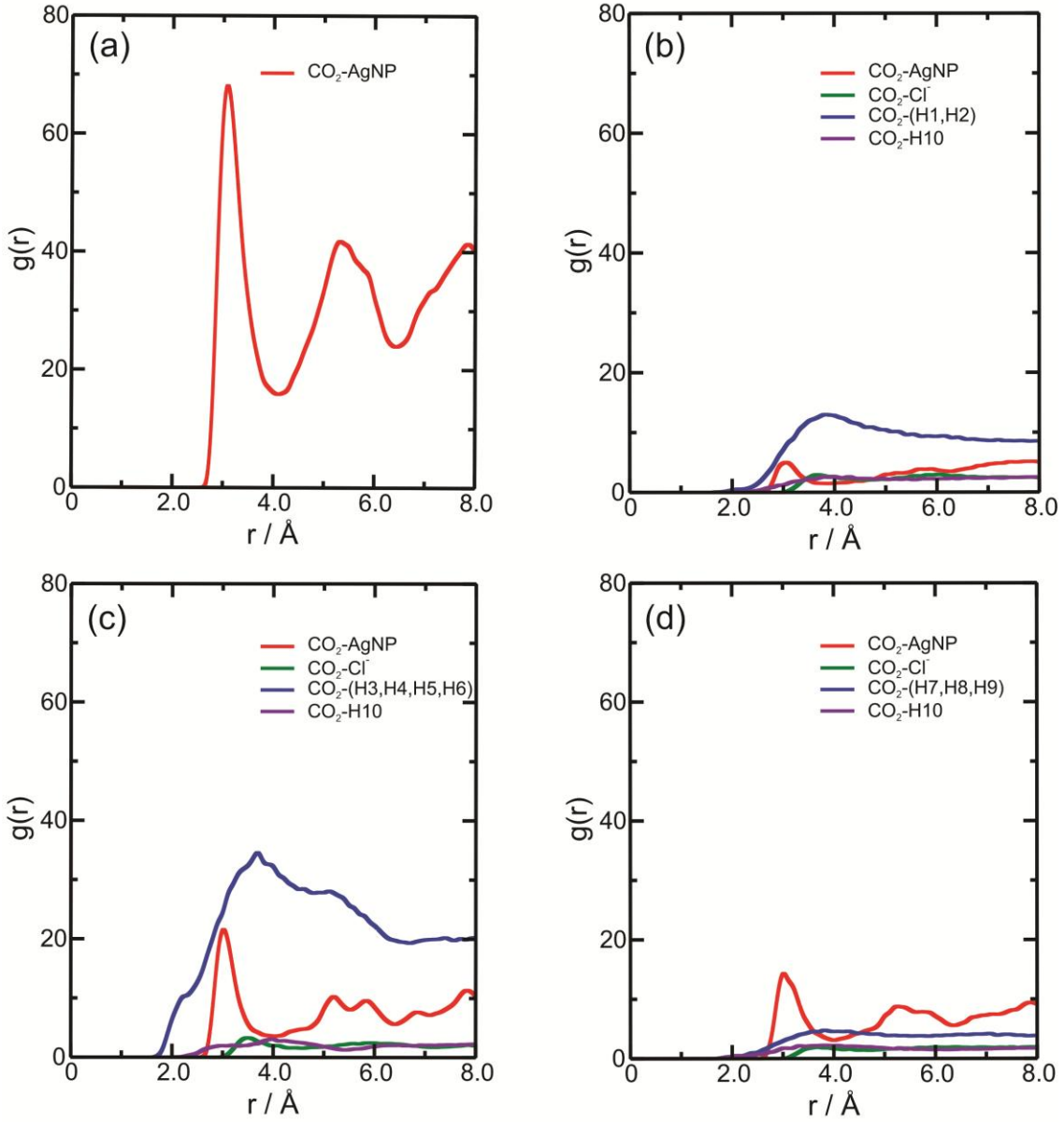

Fig. 11. RDF of (a) AgNP-CO_2, (b) AgNP-ethaline-CO_2, (c) AgNP-reline-CO_2, and (d) AgNP-glyceline-CO_2 systems.

The SDF analysis (Fig. 12) is utilized to visualize how the density components present in the system are distributed around the CO_2 molecules. For the AgNP-CO_2 system (Fig. 12a), it was observed that the CO_2 molecule is surrounded mainly by the AgNP density (violet color). Concerning the AgNP-ethaline-CO_2 system (Fig. 12b), the CO_2 molecule is surrounded mainly by chloride (green color), ethylene glycol (blue color), and AgNP densities. Posteriorly, a low density of choline (yellow color) surrounds the CO_2 molecule. On the other hand, in the AgNP-reline-CO_2 system (Fig. 12c), the CO_2 molecule was mainly surrounded by the density of urea (blue color). Furthermore, it was

observed that, in descending order of density around the CO_2 molecule, the AgNP, choline, and chloride species were observed. Concerning the AgNP-glyceline-CO_2 system (Fig. 12d), the glycerol (blue color), choline, and chloride densities surround the CO_2 molecule. However, it was also observed that AgNP and some chloride densities are more dispersed in this system.

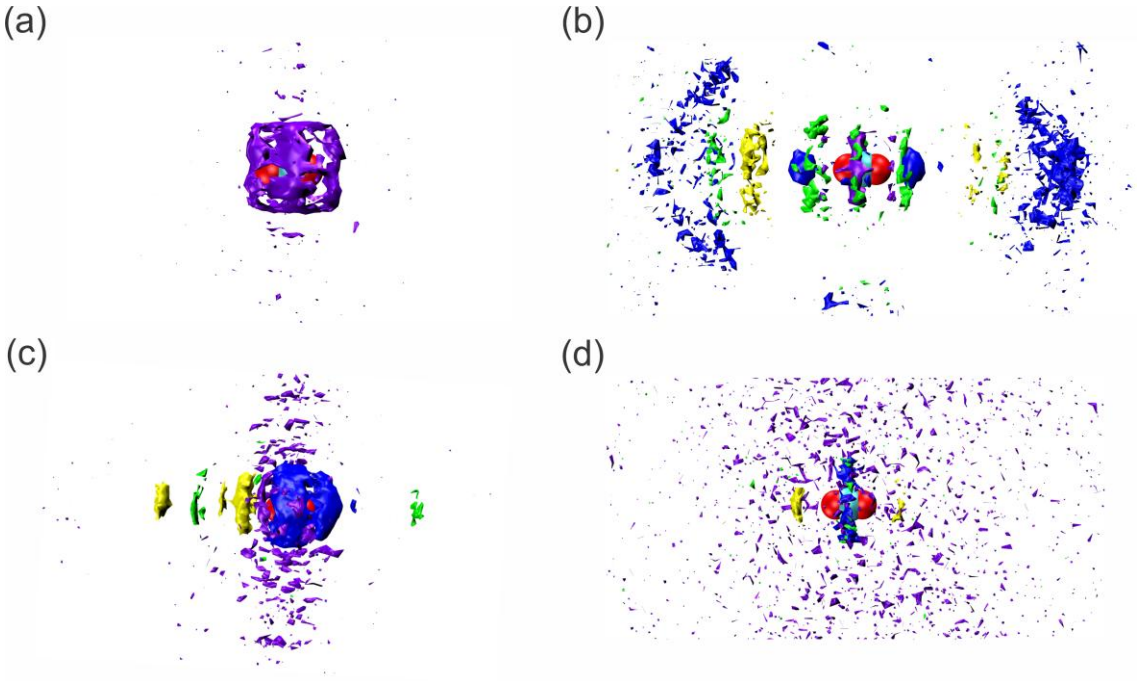

Fig. 12. SDF for the (a) AgNP-CO_2, (b) AgNP-ethaline-CO_2, (c) AgNP-reline-CO_2, and (d) AgNP-glyceline-CO_2 systems. CO_2 (van der Waals visualization); Chloride (green); ethylene glycol, urea, or glycerol (blue); choline (yellow); AgNP (violet).

3. Conclusion

The MD simulations showed that the AgNP presence in ethaline, reline, and glyceline solvents analyzed increased the HB between CO_2 molecules and the species acting as hydrogen bond donors, especially in the AgNP-reline-CO_2 system. The increased HB for these systems directly affected the IPE values, where it was observed improve in the CO_2 capture process due to a reduction of IPE values, especially for the AgNP-reline-CO_2 system compared to the AgNP-ethaline-CO_2 system and AgNP-glyceline-CO_2 system. Furthermore, the RDF analysis suggests that the ethylene glycol, urea, and AgNP species are the key species in the CO_2 capture process in the AgNP-ethaline-CO_2, AgNP-reline-CO_2, and AgNP-glyceline-CO_2 systems, respectively.

Supplementary Material

Table S6

Number of HB between the CO_2-HBD and CO_2-Ch^+ species for each replicate.

Systems	Hydrogen bonds		
	Replicate	CO_2-HBD	CO_2-Ch^+
ethaline-CO_2	1	0.67 (±0.80)	0.11 (±0.34)
	2	0.68 (±0.82)	0.17 (±0.40)
	3	0.66 (±0.80)	0.16 (±0.40)
reline-CO_2	1	3.65 (±1.84)	0.09 (±0.31)
	2	3.70 (±1.73)	0.16 (±0.38)
	3	3.97 (±1.89)	0.12 (±0.37)
glyceline-CO_2	1	1.31 (±1.22)	0.17 (±0.41)
	2	1.32 (±1.13)	0.18 (±0.42)
	3	1.26 (±1.09)	0.20 (±0.43)
AgNP-ethaline-CO_2	1	0.34 (±0.59)	0.08 (±0.28)
	2	0.31 (±0.53)	0.43 (±0.53)
	3	2.01 (±1.04)	0.04 (±0.20)
AgNP-reline-CO_2	1	5.96 (±1.91)	0.02 (±0.15)
	2	5.64 (±1.63)	0.03 (±0.16)
	3	5.17 (±1.69)	0.05 (±0.16)
AgNP-glyceline-CO_2	1	1.21 (±1.11)	0.25 (±0.48)
	2	1.35 (±1.09)	0.10 (±0.30)
	3	1.75 (±1.22)	0.07 (±0.27)

Table S7

IPE values of the three replicates between the AgNP and the DESs components for the AgNP-ethaline-CO_2, AgNP-reline-CO_2, and AgNP-glyceline-CO_2 systems.

Interaction potential energy / kJ mol^{-1}					
Systems / Interactions	Replicates	HBD-AgNP	Ch^+-AgNP	Cl^--AgNP	DESs-AgNP
AgNP-ethaline-CO_2	1	-6241.51 (±119.22)	-2882.50 (±72.98)	-349.82 (±17.70)	-9473.83
	2	-6069.98 (±123.41)	-2843.34 (±78.75)	-359.13 (±16.58)	-9272.45
	3	-6042.17 (±125.75)	-2860.64 (±71.37)	-319.77 (±16.81)	-9222.58
AgNP-reline-CO_2	1	-5975.68 (±177.61)	-3002.30 (±90.32)	-477.08 (±16.82)	-9455.06
	2	-5832.23 (±178.96)	-3207.43 (±74.07)	-522.49 (±20.68)	-9562.15
	3	-5767.32 (±176.48)	-3221.12 (±77.93)	-512.85 (±16.09)	-9501.29
AgNP-glyceline-CO_2	1	-6910.38 (±47.45)	-2151.67 (±35.36)	-241.42 (±14.18)	-9303.47
	2	-6844.99 (±46.02)	-2173.97 (±33.60)	-230.73 (±11.67)	-9249.69
	3	-6991.16 (±48.67)	-2108.85 (±38.11)	-244.35 (±11.51)	-9344.36

Table S8

IPE values of the first replicate between the CO_2 molecules and the species in all the simulated systems.

	Interaction potential energy / kJ mol^{-1}						
Systems / Interactions	CO_2-CO_2	CO_2-AgNP	CO_2-Cl^-	CO_2-HBD	CO_2-Ch^+	CO_2-DESs	CO_2-DESs-AgNP
ethaline-CO_2	-7.58 (±1.49)		-16.07 (±14.93)	-208.04 (±27.82)	-195.88 (±22.94)	-419.99	
reline-CO_2	-8.45 (±2.93)		-31.78 (±21.38)	-245.74 (±36.79)	-260.12 (±29.61)	-537.64	
glyceline-CO_2	-7.26 (±6.59)		-12.11 (±13.65)	-232.50 (±31.63)	-162.10 (±21.83)	-406.71	
AgNP-CO_2	-11.60 (±3.18)	-1098.32 (±29.49)					
AgNP-ethaline-CO_2	-5.61 (±1.10)	-90.76 (±20.95)	-16.52 (±14.16)	-243.95 (±22.02)	-236.44 (±19.68)	-496.91	-587.67
AgNP-reline-CO_2	-5.85 (±1.33)	-265.15 (±13.17)	-11.90 (±10.07)	-297.71 (±21.28)	-198.96 (±15.02)	-508.57	-773.72
AgNP-glyceline-CO_2	-5.80 (±1.78)	-222.21 (±26.24)	-11.60 (±11.95)	-266.52 (±24.25)	-177.23 (±17.43)	-455.35	-677.56

Table S9

IPE values of the second replicate between the CO_2 molecules and the species in all the simulated systems.

	Interaction potential energy / kJ mol^{-1}						
Systems / Interactions	CO_2-CO_2	CO_2-AgNP	CO_2-Cl^-	CO_2-HBD	CO_2-Ch^+	CO_2-DESs	CO_2-DESs-AgNP
ethaline-CO_2	-7.64 (±2.99)		-16.03 (±15.39)	-208.56 (±27.68)	-196.22 (±23.69)	-420.81	
reline-CO_2	-5.97 (±2.07)		-27.52 (±16.47)	-269.24 (±30.14)	-262.89 (±24.35)	-559.65	
glyceline-CO_2	-7.28 (±2.97)		-11.29 (±13.75)	-231.19 (±31.69)	-160.72 (±22.52)	-403.20	
AgNP-CO_2	-13.16 (±3.39)	-1084.75 (±28.60)					
AgNP-ethaline-CO_2	-5.72 (±1.77)	-301.52 (±13.38)	-15.07 (±13.11)	-232.39 (±21.43)	-206.66 (±17.53)	-454.12	-755.64
AgNP-reline-CO_2	-10.29 (±2.03)	-211.51 (±8.51)	-43.60 (±11.19)	-297.71 (±19.08)	-202.11 (±13.04)	-543.42	-754.93
AgNP-glyceline-CO_2	-7.48 (±2.72)	-252.34 (±19.43)	-21.79 (±15.05)	-266.52 (±24.25)	-164.21 (±20.20)	-452.44	-704.78

Table S10

IPE values of the third replicate between the CO_2 molecules and the species in all the simulated systems.

Interaction potential energy / kJ mol^{-1}							
Systems / Interactions	CO_2-CO_2	CO_2-AgNP	CO_2-Cl^-	CO_2-HBD	CO_2-Ch^+	CO_2-DESs	CO_2-DESs-AgNP
ethaline-CO_2	-7.53 (±2.80)		-15.83 (±15.39)	-208.24 (±28.93)	-197.78 (±23.81)	-421.85	
reline-CO_2	-10.15 (±4.55)		-27.61 (±17.08)	-246.88 (±32.26)	-254.84 (±29.29)	-529.33	
glyceline-CO_2	-7.32 (±6.59)		-12.11 (±13.33)	-229.94 (±30.76)	-162.48 (±21.40)	-404.53	
AgNP-CO_2	-13.65 (±3.69)	-1077.13 (±29.77)					
AgNP-ethaline-CO_2	-4.47 (±2.07)	-353.39 (±16.37)	-32.93 (±13.42)	-216.42 (±22.97)	-195.94 (±17.16)	-445.29	-798.68
AgNP-reline-CO_2	-7.68 (±1.72)	-229.45 (±9.47)	-50.83 (±11.69)	-258.98 (±18.76)	-205.13 (±13.77)	-514.94	-744.39
AgNP-glyceline-CO_2	-5.47 (±1.26)	-185.83 (±29.46)	-15.63 (±15.05)	-273.37 (±27.93)	-170.58 (±17.11)	-459.58	-645.41

4 CONCLUSIONS

In this PhD thesis, two works about CO_2 capture were developed. The first work, "Analysis of temperature in the CO_2 absorption using a deep eutectic solvent: an in silico approach", was realized through MD simulations and NCI calculations. The MD simulations indicated the increased effect temperature occasioned in the reduction of HB number between the CO_2 and U species, occasioning in an increase of IPE values for this interaction. Besides, the RDF analysis suggested the increased effect temperature reduces the probability density of CO_2 molecules interacting with other species of DESs. On the other hand, the solvation layer of CO_2 was not affected. NCI simulations indicated that the increased temperature resulted in the repulsion interactions and reduced the strong interactions. Therefore, both computational approaches indicated the CO_2 absorption process is more indicated at the temperature of 303 K.

The second work, "Synergic effect of Ag nanoparticles and deep eutectic solvents in the CO_2 capture process: a computational approach", was simulated through MD simulations. The MD results indicated that the AgNP presence in three DESs increased the HB number of CO_2-E, CO_2-U, and CO_2-G groups, especially for the CO_2-U group. This increase of HB directly affected the average IPE values for these groups, occasioning the reduction of these average IPE values, resulting in an improvement of the CO_2 capture process, especially for the AgNP-reline-CO_2 system. Furthermore, the RDF analysis suggested that ethylene glycol and urea are key species in the CO_2 capture for the AgNP-reline-CO_2 and AgNP-reline-CO_2 systems, respectively. On the other hand, the AgNP is the key specie in the CO_2 capture for the AgNP-glyceline-CO_2 system.

REFERENCES

ABO-HAMAD, Ali et al. Potential applications of deep eutectic solvents in nanotechnology. **Chemical Engineering Journal**, v. 273, p. 551–567, 2015.

ABRAHAM, Mark J. et al. GROMACS: High performance molecular simulations through multi-level parallelism from laptops to supercomputers. **SoftwareX**, v. 1–2, p. 19–25, 2015.

AHMAD, Tausif et al. Performance evaluation of phosphonium based deep eutectic solvents coated cerium oxide nanoparticles for CO_2 capture. **Environmental Research**, v. 222, p. 115314, 2023.

AKBARI, Mahmood; MORAD, Razieh; MAAZA, Malik. Effect of silver nanoparticle size on interaction with artemisinin: First principle study. **Results in Surfaces and Interfaces**, v. 11, n. 8, p. 100104, 2023.

AMORIM-CARMO, Bruno et al. Potent and Broad-Spectrum Antimicrobial Activity of Analogs from the Scorpion Peptide Stigmurin. **International journal of molecular sciences**, v. 20, n. 3, 2019.

ÅSTRÖM, Daniel et al. Evolution of minimum mortality temperature in Stockholm, Sweden, 1901-2009. **Environmental Health Perspectives**, v. 124, n. 6, p. 740–744, 2016.

BALASUBRAMANIAM, Bhubesh et al. Process-performance of solid sorbents for Direct Air Capture (DAC) of CO_2 in optimized temperature-vacuum swing adsorption (TVSA) cycles. **Chemical Engineering Journal**, v. 485, p. 149568, 2024.

BERENDSEN, Herman et al. Molecular dynamics with coupling to an external bath. **The Journal of Chemical Physics**, v. 81, n. 8, p. 3684–3690, 1984.

BEZERRA, Lucas et al. Analysis of temperature effect in the CO_2 absorption using a deep eutectic solvent: An in silico approach. **Journal of Molecular Graphics and Modelling**, v. 126, p. 108649, 2024.

BEZERRA, Lucas et al. Electrochemical and theoretical investigation on the behavior of the Co^{2+} ion in three eutectic solvents. **Journal of Molecular Graphics and Modelling**, v. 112, p. 108137, 2022.

BUSSI, Giovanni; DONADIO, Davide; PARRINELLO, Michele. Canonical sampling through velocity rescaling. **The Journal of chemical physics**, v. 126, n. 1, 2007.

CHAI, Jeng-Da.; HEAD-GORDON, Martin. Long-range corrected hybrid density functionals with damped atom–atom dispersion corrections. **Physical Chemistry Chemical Physics**, v. 10, p. 6615–6620, 2008.

CHANG, Kuan et al. Improving CO_2 Electrochemical Reduction to CO Using Space Confinement between Gold or Silver Nanoparticles. T**he Journal of Physical Chemistry** Letters, v. 11, n. 5, p. 1896–1902, 2020.

CHOI, Yeol et al. CHARMM-GUI Nanomaterial Modeler for Modeling and Simulation of Nanomaterial Systems. **Journal of Chemical Theory and Computation**, v. 18, n. 1, p. 479–493, 2021.

CHUN, Sangki et al. Roll-to-Roll Printing of Silver Oxide Pastes and Low Temperature Conversion to Silver Patterns. **Chemistry of Materials**, v. 21, n. 2, p. 343–350, 2008.

DUTCHER, Bryce; FAN, Maohong; RUSSELL, Armistead. Amine-Based CO_2 Capture Technology Development from the Beginning of 2013—A Review. **ACS Applied Materials and Interfaces**, v. 7, n. 4, p. 2137–2148, 2015.

FRISCH, Michael. et al. Gaussian 09, Revision B.01Gaussian 09, Revision B.01, Gaussian, Inc., Wallingford CT Wallingford CT, 2009.

FRISCH, Michael; POPLE, John; BINKLEY, John. Stephen. Self-consistent molecular orbital methods 25. Supplementary functions for Gaussian basis sets. **The Journal of Chemical Physics**, v. 80, n. 7, p. 3265–3269, 1984.

GARCÍA, Gregorio; ATILHAN, Mert; APARICIO, Santiago. The impact of charges in force field parameterization for molecular dynamics simulations of deep eutectic solvents. **Journal of Molecular Liquids**, v. 211, p. 506–514, 2015.

GARCÍA-LOJO, Daniel et al. The role of deep eutectic solvents and carrageenan in synthesizing biocompatible anisotropic metal nanoparticles. **Beilstein Journal of Nanotechnology**, v. 12, n. 7, p. 924–938, 2021.

GREENMATCH. Countries with the highest carbon footprint 2025. Disponível em: <https://www.greenmatch.co.uk/blog/countries-with-the-highest-carbonfootprint>.

HAUG, Edward; ARORA, Jasbir; MATSUI, Kanae. A steepest-descent method for optimization of mechanical systems. **Journal of Optimization Theory and Applications**, v. 19, n. 3, p. 401–424, 1976.

HE, Ting et al. Thermodynamic optimization and exergy analysis of a combined cryogenic CO_2 capture process for hydrogen production via steam methane reforming. **Fuel**, v. 400, p. 135750, 2025.

IZGORODINA, Ekaterina; MACFARLANE, Douglas. Nature of Hydrogen Bonding in Charged Hydrogen-Bonded Complexes and Imidazolium-Based Ionic Liquids. **Journal of Physical Chemistry B**, v. 115, n. 49, p. 14659–14667, 2011.

JO, Sunhwan et al. CHARMM-GUI: A web-based graphical user interface for CHARMM. **Journal of Computational Chemistry**, v. 29, n. 11, p. 1859–1865, 2008.

JOHNSON, Erin et al. Revealing Noncovalent Interactions. **Journal of the American Chemical Society**, v. 132, n. 18, p. 6498–6506, 2010.

JONES, Matthew et al. National contributions to climate change due to historical emissions of carbon dioxide, methane, and nitrous oxide since 1850. **Scientific Data**, v. 10, n. 1, p. 155-, 2023.

JORGENSEN, William; TIRADO-RIVES, Julian. The OPLS [optimized potentials for liquid simulations] potential functions for proteins, energy minimizations for crystals of cyclic peptides and crambin. **Journal of the American Chemical Society**, v. 110, n. 6, p. 1657–1666, 1988.

JSCITECHNOL, Indian; VENKATARAMANAN, M. Causes and effects of global warming. **Indian Journal of Science and Technology**, v. 4, n. 3, p. 226–229, 2011.

KANG, Wen et al. Ultrafine Ag Nanoparticles as Active Catalyst for Electrocatalytic Hydrogen Production. **ChemCatChem**, v. 11, n. 24, p. 5976–5981, 2019.

KIM, Seonghoon et al. CHARMM-GUI ligand reader and modeler for CHARMM force field generation of small molecules. **Journal of Computational Chemistry**, v. 38, n. 21, p. 1879–1886, 2017.

KRZYWANSKI, Jaroslaw et al. NOx Emissions from Regenerator of Calcium Looping Process. **Energy & Fuels**, v. 32, n. 5, p. 6355–6362, 2018.

KUSSAINOVA, Dina; SHAH, Dhawal. Monoethanolamine based DESs for CO_2 absorption: Insights from molecular dynamics simulations. **Separation and Purification Technology**, v. 231, p. 115931, 2020.

LEE, Jumin et al. CHARMM-GUI Input Generator for NAMD, GROMACS, AMBER, OpenMM, and CHARMM/OpenMM Simulations Using the CHARMM36 Additive Force Field. **Journal of Chemical Theory and Computation**, v. 12, n. 1, p. 405–413, 2015.

LERON, Rhoda; CAPARANGA, Alvin; LI, Hui. Carbon dioxide solubility in a deep eutectic solvent based on choline chloride and urea at T = 303.15–343.15 K and moderate pressures. **Journal of the Taiwan Institute of Chemical Engineers**, v. 44, n. 6, p. 879–885, 2013.

LÓPEZ-CARBALLO, Gracia et al. Silver Ions Release from Antibacterial Chitosan Films Containing in Situ Generated Silver Nanoparticles. **Journal of Agricultural and Food Chemistry**, v. 61, n. 1, p. 260–267, 2012.

LU, Tian; CHEN, Feiwu. Multiwfn: A multifunctional wavefunction analyzer. **Journal of Computational Chemistry**, v. 33, n. 5, p. 580–592, 2012.

MANSUROV, Ulan et al. Particulate Matter Formation in Post-combustion CO_2 Capture Columns: Insights from Molecular Dynamics Simulations. **Energy & Fuels**, v. 32, n. 12, p. 12679–12688, 2018.

MICARI, Marina; Dakhchoune, Mostapha; AGRAWAL, Kumar. Techno-economic assessment of postcombustion carbon capture using high-performance nanoporous single-layer graphene membranes. **Journal of Membrane Science**, v. 624, p. 119103, 2021.

MJALLI, Farouq et al. Monoethanolamine-based deep eutectic solvents, their synthesis and characterization. **Fluid Phase Equilibria**, v. 448, p. 30–40, 2017.

MOOSAVI, Fatemeh; ABDOLLAHI, Farkhondeh; RAZMKHAH, Mohammad. Carbon dioxide in monoethanolamine: Interaction and its effect on structural and dynamic properties by molecular dynamics simulation. **International Journal of Greenhouse Gas Control**, v. 37, p. 158–169, 2015.

MUSKALA, Waldemar; KRZYWANSKI, J. The research of CFB boiler operation for oxygenenhanced dried lignite combustion. **Rynek Energii**, v. 92, n. 1, p. 172 – 176, 2011.

NATIONAL OCEANIC AND ATMOSPHERIC ADMINISTRATION (NOAA). Trends in atmospheric carbon dioxide (CO_2). NOAA Global Monitoring Laboratory. Disponível em: <https://gml.noaa.gov/ccgg/trends/>.

NAVAS-MARTÍN, Miguel et al. Population adaptation to heat as seen through the temperature-mortality relationship, in the context of the impact of global warming on health: A scoping review. **Science of The Total Environment**, v. 908, p. 168441, 2024.

NAWAZ KHAN, Saleem et al. Preparation of ionic liquids amine hybrid solvents, characterization for CO_2 absorption, and kinetic performance. **Journal of Molecular Liquids**, v. 394, p. 123725, 2024.

NEWMAN, Rebecca; NOY, Ilan. The global costs of extreme weather that are attributable to climate change. **Nature Communications**, v. 14, n. 1, p. 6103-, 2023.

NGUYEN, Dang et al. Electrochemical conversion of carbon dioxide over silver-based catalysts: Recent progress in cathode structure and interface engineering. **Chemical Engineering Science**, v. 234, p. 116403, 2021.

NOORANI, Narmin et al. Improved the CO_2 adsorption performance in cobalt oxide nanoparticles in the presence of DES. **New Journal of Chemistry**, v. 47, n. 35, p. 16748–16755, 2023.

PARRINELLO, Michele; RAHMAN, Aneesur. Polymorphic transitions in single crystals: A new molecular dynamics method. **Journal of Applied Physics**, v. 52, n. 12, p. 7182–7190, 1981.

PERDEW, John; BURKE, Kieron; ERNZERHOF, Matthias. Generalized Gradient Approximation Made Simple. **Physical Review Letters**, v. 77, n. 18, p. 3865, 1996.

SHAH, Dhawal et al. Molecular dynamics simulations on extractive desulfurization of fuels by tetrabutylammonium chloride based Deep Eutectic Solvents. **Journal of Molecular Liquids**, v. 274, p. 254–260, 2019.

SMITH, Emma; ABBOTT, Andrew; RYDER, Karl. Deep Eutectic Solvents (DESs) and Their Applications. **Chemical Reviews**, v. 114, n. 21, p. 11060–11082, 2014.

YAASHIKAA, Ponnambalam et al. A review on photochemical, biochemical and electrochemical transformation of CO_2 into value-added products. **Journal of CO_2 Utilization**, v. 33, p. 131–147, 2019.

YUAN, Gonglin; LI, Tingting; HU, Wujie. A conjugate gradient algorithm and its application in large-scale optimization problems and image restoration. **Journal of Inequalities and Applications**, v. 2019, n. 1, p. 247-, 2019.

ZYLKA, Anna et al. The 4th Generation of CeSFaMB in numerical simulations for CuO-based oxygen carrier in CLC system. **Fuel**, v. 255, p. 115776, 2019.

APPENDIX A – CURRICULUM SUMMARY

Education

Ph.D. in Chemistry

Federal University of Ceará March 2022 - January 2026

Thesis: Computational analysis of CO_2 capture through deep eutectic solvents and silver nanoparticles

Supervisors: Dr. Norberto de Kássio Vieira Monteiro and Dr. Adriana Nunes Correia

M.Sc. in Chemistry

Federal University of Ceará August 2019 - Dezember 2021

Thesis: Electrochemical and theoretical investigation on the behavior of the Co^{2+} ion in three eutectic solvents

Supervisor: Dr. Norberto de Kássio Vieira Monteiro

B.Sc. in Chemistry

State University of Ceará August 2014 - Dezember 2018

Thesis: *In silico* evaluate of pharmacology potential of carotenoids present in bixa orellana against the dengue virus

Supervisor: Dr. Emmanuel Silva Marinho

Scholarships, Awards, and Grants

SCHOLARSHIPS

2022-2026 **Graduate research scholarship:** Academic Excellence Program, CAPES, Br.

2018-2021 **Graduate research scholarship:** Academic Excellence Program, CAPES, Br.

2017-2018 **Undergraduate research scholarship:** Academic Excellence Program, CNPQ, Br.

2016-2017 **Undergraduate research scholarship:** Academic Excellence Program, FUNCAP, Br.

AWARDs & GRANTS

2024 - 2025 **Visiting P.hD. Program grant:** for a research stay of six months at the Porto

Polytechnic Institute.

2017 Honorable Mention at the 57º Brazilian Journey of Scientific Initiation in Chemistry.

Publications

[1] M. Tavares, **L. Bezerra**, C. Delerue-Matos, A. Correia, N. Monteiro, A. Torrinha, S. Morais, Carbon paper/copper metal-organic framework sensor for detection of the European Union watch list substance metformin: electroanalysis and computational mechanistic insights, Sensors And Actuators Reports 11 (2026) 100426. https://doi.org/10.1016/j.snr.2025.100426

[2] C. L. Peixoto, V. K. F. Monteiro, J.O. de Souza Júnior, **L.L. Bezerra**, G. M. C. de Castro, N. de K. V. Monteiro, R. A. Moreira, A. M. A. Martins, L. Belayev, R. B. Oriá, The Antithrombotic Potential of Sulfated-Polysaccharides from Red Seaweed Hypnea musciformis (Wulfen) J.V. Lamouroux: An In Vitro, In Silico and In Vivo Study, ACS Omega 11 (2026) 5181. https://doi.org/10.1021/acsomega.5c07355

[3] **L.L. Bezerra**, P. de Lima-Neto, A.N. Correia, N. de K. Vieira Monteiro, Synergy effect of Ag nanoparticles and deep eutectic solvents in the CO_2 capture process: A computational approach, Journal of Molecular Liquids 417 (2025) 126517. https://doi.org/10.1016/j.molliq.2024.126517

[4] G. N. Castro, **L. L. Bezerra**, L. P. da Silva, P. de Lima-Neto, A. N. Correia, N. K. V. Monteiro, Computational study of water adsorption on iron surfaces and metallic alloys, Journal of Molecular Liquids 433 (2025) 127973. https://doi.org/10.1016/j.molliq.2025.127973

[5] N. G. Sousa, **L.L. Bezerra**, K.L. Gomes, F.X. Feitosa, H.B. de Sant'Ana, L.H. Mascaro, W. Schwarzacher, P. de Lima-Neto, N.K.V. Monteiro, P.N.S. Casciano, A.N. Correia, NiMo electrocatalysts from a deep eutectic solvent for the hydrogen evolution reaction, International Journal of Hydrogen Energy 142 (2025) 130. https://doi.org/10.1016/j.ijhydene.2025.05.272

[6] J.O. de Souza Júnior, N.G. Sousa, R.V. de Oliveira, **L.L. Bezerra**, P.N. da S. Casciano, A.N. Correia, P. de L. Neto, N. de K.V. Monteiro, Theoretical and experimental insights of two surfactants' effects on SnIn electrodeposited coatings from ethaline, Journal of Molecular Structure 1323 (2025) 140668. https://doi.org/10.1016/j.molstruc.2024.140668

[7] **L.L. Bezerra**, A.N. Correia, P. de Lima-Neto, N. de K.V. Monteiro, Analysis of

Temperature Effect in the CO_2 Absorption Using a Deep Eutectic Solvent: An in Silico Approach, Journal of Molecular Graphics and Modelling 126 (2024) 108649. https://doi.org/10.1016/j.jmgm.2023.108649

[8] N. de K.V. Monteiro, **L.L. Bezerra**, L.P. da Silva, R. Machado, Molecular Nanoinformatics Approach Assessing the Coating Oxcarbazepine (OXC) Drug on Silver Nanoparticles, ACS Omega 9 (2024) 46091–46103. https://doi.org/10.1021/acsomega.4c06366

[9] A. Francisca T. Gomes, W.F. de Medeiros, **L.L. Bezerra**, A. Beatriz S. Luz, F.C. de Sousa Junior, S.H. de L. Vale, E.A. dos Santos, N. de K. V. Monteiro, A. Heloneida de A. Morais, Interaction between insulin receptor and a peptide derived from a trypsin inhibitor purified from tamarind seed: An in silico screening of insulin-like peptides, Arabian Journal of Chemistry 17 (2024) 105780. https://doi.org/10.1016/j.arabjc.2024.105780

[10] A.B.S. Luz, A.F. de Medeiros, **L.L. Bezerra**, M.S.R. Lima, A.S. Pereira, E.G.O. e Silva, T.S. Passos, N. de K.V. Monteiro, A.H. de A. Morais, Prospecting native and analogous peptides with anti-SARS-CoV-2 potential derived from the trypsin inhibitor purified from tamarind seeds, Arabian Journal of Chemistry 16 (2023) 104886. https://doi.org/10.1016/j.arabjc.2023.104886

[11] D.M.L. Pinheiro, **L.L. Bezerra**, A.A.C. Alcanfor, F.X. Feitosa, N.K.V. Monteiro, A.N. Correia, P. de Lima Neto, H.B. de Sant'Ana, Ag^{+} ion in choline chloride and glycerol mixture: Evaluation of electrochemical properties and molecular modelling approaches, Journal of Molecular Liquids 371 (2023) 121053. https://doi.org/10.1016/j.molliq.2022.121053

[12] L. Amorim, R.V. de Oliveira, **L.L. Bezerra**, L.P. Coutinho, P.B.A. Fechine, A.N. Correia, Á.R.L. da Silva, P. de Lima-Neto, N.K. de V. Monteiro, Analysis of Fe^{2+} and Mn^{2+} ions in DES and water: A theoretical study using molecular dynamic simulations, QTAIM and NCI-RDG, Colloids and Surfaces A: Physicochemical and Engineering Aspects 674 (2023) 131818. https://doi.org/10.1016/j.colsurfa.2023.131818

[13] L.P. da Silva, F.W.Q. Almeida-Neto, **L.L. Bezerra**, J. Silva, N.K.V. Monteiro, M.M. Marinho, H.S. dos Santos, A.M.R. Teixeira, E.S. Marinho, P. de Lima-Neto, Sulfonamide derived from anacardic acid as potential antichagasic: a theoretical approach based on molecular docking, molecular dynamics, and density functional theory calculations, Journal of Molecular Modeling 29 (2023). https://doi.org/10.1007/s00894-023-05566-9

[14] N. de K.V. Monteiro, **L.L. Bezerra**, R.J. de A. Machado, Modeling the adsorption mechanism of 3-tertiary-butyl-4-hydroxyanisole (3BHA) on polyethylene and polypropylene microplastics, Chemical Papers 78 (2023) 2359–2367. https://doi.org/10.1007/s11696-023-03243-y

[15] **L.L. Bezerra**, F.G.S. Oliveira, L.P.M. dos Santos, H.B. de Sant'Ana, F.X. Feitosa, A.N. Correia, W. Schwarzacher, E.S. Marinho, P. de Lima-Neto, N. de K.V. Monteiro, Electrochemical and theoretical investigation on the behavior of the Co^{2+} ion in three eutectic solvents, Journal of Molecular Graphics and Modelling 112 (2022) 108137. https://doi.org/10.1016/j.jmgm.2022.108137

[16] D.R. Moreira, E.N. Ferreira, J.F.C. Neto, **L.L. Bezerra**, N. de K.V. Monteiro, C.P. do Valle, T.B.M.G. Arruda, P. de Lima Neto, J.S. Rodrigues, F.E.A. Rodrigues, C.L. Petzhold, M.E. Maier, N.M.P.S. Ricardo, Green lubricants production from Nile tilapia waste and prediction of physical properties through molecular dynamics simulations, Journal of the American Oil Chemists' Society 99 (2022) 341–352. https://doi.org/10.1002/aocs.12580

[17] I. Costa, M. Lima, A. Medeiros, **L. Bezerra**, P. Santos, A. Serquiz, M. Lima, G. Oliveira, E. Santos, B. Maciel, N. Monteiro, A.H. Morais, An Insulin Receptor-Binding Multifunctional Protein from Tamarindus indica L. Presents a Hypoglycemic Effect in a Diet-Induced Type 2 Diabetes—Preclinical Study, Foods 11 (2022) 2207. https://doi.org/10.3390/foods11152207

[18] R.V. de Oliveira, **L.L. Bezerra**, N.G. Sousa, F.X. Feitosa, H.B. de Sant'Ana, A.N. Correia, P. de Lima-Neto, N.K.V. Monteiro, Analysis of the behavior of Sn^{2+} and In^{3+} ions in DES and in water: A theoretical approach, Journal of Molecular Liquids 353 (2022) 118774. https://doi.org/10.1016/j.molliq.2022.118774

[19] M.R. Xavier, T.S. Freitas, R.L.S. Pereira, E.M. Marinho, P.N. Bandeira, A.P. de Sousa, L.S. Oliveira, **L.L. Bezerra**, J.B.A. Neto, M.M.C. Silva, B.G. Cruz, J.E. Rocha, C.R.S. Barbosa, A.W. da Silva, J.E.S.A. de Menezes, H.D.M. Coutinho, M.M. Marinho, E.S. Marinho, H.S. dos Santos, A.M.R. Teixeira, Anti-inflammatory effect, antibiotic potentiating activity against multidrug-resistant strains of Escherichia coli and Staphylococcus aureus, and evaluation of antibiotic resistance mechanisms by the ibuprofen derivative methyl 2-(-4-isobutylphenyl)propanoate. Microbial Pathogenesis 170 (2022) 105697. https://doi.org/10.1016/j.micpath.2022.105697

[20] **L.L. Bezerra**, F.W.Q. Almeida-Neto, M.M. Marinho, L. Santos Oliveira, A.M.R. Teixeira, P.N. Bandeira, H.S. dos Santos, P. de Lima-Neto, E.S. Marinho, Synthesis of

aminochalcones and in silico evaluation of their antiparasitic potential against Leishmania, Journal of Biomolecular Structure and Dynamics 41 (2022) 6434–6441. https://doi.org/10.1080/07391102.2022.2103030

[21] J.R. Bezerra-Neto, **L.L. Bezerra**, N.G. Sousa, L.P.M. dos Santos, E.S. Marinho, N.K.V. Monteiro, A.N. Correia, P. de Lima-Neto, Molecular approach about the effect of water on the electrochemical behaviour of Ag^{+} ions in urea-choline chloride-water mixture, Journal of Molecular Modeling 26 (2020). https://doi.org/10.1007/s00894-020-04587-y